containing 0.25 mM dNTP mixture, 0.5 μM each primer and 1.0 U of Hot Start *Taq* polymerase (TaKaRa). Touchdown PCR was then carried out using the primer sequences and restriction enzymes listed in Table 2. Primers were designed based on the nucleotide sequences obtained from Genbank (AC023047). Samples (20 μl) of PCR product were digested with restriction enzymes that cleave CpG sites retained because of methylation. After ethanol precipitation, the DNA was subjected to 3% agarose gel electrophoresis and stained with ethidium bromide.

Sequence analysis

To sequence bisulfite-PCR products, fragments amplified using primer CIITAGM1-F and SeqR-R were cloned into pCR4 vector using a TOPO-cloning Kit (Invitrogen), after which plasmid DNA was purified using an automated DNA purification system (PI100, Kurabo, Tokyo, Japan). To perform direct sequencing, amplified RT-PCR products were electrophoresed in 1% Seaplaque gels, excised and purified using a PCR Purification System (Promega). The cycle sequencing reaction was carried out using a BigDye terminator kit, after which the DNA was sequenced using an ABI 3100 automated sequencer (Applied Biosystems).

RT-PCR

Total RNA was prepared from samples of gastric and colorectal cancer cell lines, after which 5-μg samples were reverse-transcribed using Superscript II (Invitrogen) to prepare first-strand cDNA. Primer sequences and PCR parameters are shown in Table 2. To separately amplify the three CIITA isoforms, primers were designed based on the sequences of CIITA-PI, -PIII and -PIV (AF000002, AF000003, AF000004), as shown in Figure 3a. Controls consisted of RNA treated identically but without the addition of reverse transcriptase and are labeled as RT-. The integrity of the cDNA was confirmed by amplifying GAPDH as described previously (Suzuki *et al*., 2000). Samples (10 μl) of amplified product were subjected to 2.5% agarose gel electrophoresis and stained with ethidium bromide.

Western blot analysis

Cells were lysed in ice-cold Tris buffer (20 mM Tris, pH 7.5) containing 137 mM NaCl, 2 mM EDTA, 1% Triton X, 10% glycerol, 50 mM NaF, 1 mM DTT and a protease inhibitor cocktail (Roche Applied Science). A measure of 20 μg of cell lysate was then separated by 10% SDS–PAGE, transferred to

Table 2 Primer sequences for bisulfite-PCR, RT-PCR and ChIP analysis

	Sequence	*Annealing temperature (°C)*	*Enzyme, size (bp)*
Bisulfite-PCR			
GM1 (region 2)	F: 5′-GTAGTTGGGATGTTATTTTTGATAAAG-3′ R: 5′-TCTCCCTCCCRCCAACTCT-3′	58 (3), 56 (4), 54 (5), 52 (26)	TaqI, BstUI 195
GM2 (region 3)	F: 5′-GGTTATATAGTAAGTTTGGGAGGATG-3′ R: 5′-CRACCCCRAAACTCTAAACAC-3′	58 (3), 56 (4), 54 (5), 52 (26)	BstUI, HinfI 155
GM3 (region 4)	F: 5′-GTGGGYGGGTGGTAGGAAAG-3′ R: 5′-AAACTCAAAAAACRACRACCCTAATC-3′	58 (3), 56 (4), 54 (5), 52 (26)	TaqI, TaiI 184
GM4 (region 1)	F: 5′-TAGGAATTTAAGATTTTTGAAAAGGA-3′ R: 5′-RAAAACACATAACCCCTAAAATAAAC-3′	58 (3), 56 (4), 54 (5), 52 (26)	MboI 179
SeqR	5′-ACAATCTCRAAACCTCRATTCTC-3′	58 (3), 56 (4), 54 (5), 52 (26)	
RT–PCR			
C2TA-PIV	F: 5′-AGACTTGCCGCGGCCCCAGAG-3′ R: 5′-GTAGAGGCACAGGGGGTCAGC-3′	68 (3), 66 (4), 64 (5), 62 (26)	157
CIITA-PI	F: 5′-ACTTCCAGGCCATCCTGACT-3′ R: 5′-GTAGAGGCACAGGGGGTCAGC-3′	70 (3), 68 (4), 66 (5), 64 (26)	368
CIITA-PIII	F: 5′-TTCCTACACAATGCGTTGCC-3′ R: 5′-TGCTGAACTGGTCGCAGTTGATGG-3′	70 (3), 68 (4), 66 (5), 64 (26)	225
RT-HLA-DR	F: 5′-GCCAACCTGGAAATCATGACA-3′ R: 5′-AGGGCTGTTCGTGAGCACA-3′	55 (35)	86
IRF-1	F: 5′-GCTCCACTCTGCCTGATGACCAC-3′ R: 5′-GCTGTCAATTTCTGGCTCCTCCTTA-3′	62 (32)	386
RFX-5	F: 5′-AACCACCTGGAAGAGCACACTGAC-3′ R: 5′-CCAGGCAGGGGTGGCATAGA-3′	60 (35)	239
RFX-AP	F: 5′-GTGCAAGAAACACCGCAACAAGAT-3′ R: 5′-CTGCTGTTGTCTTTGCTCCAAAACT-3′	60 (35)	316
HPP1/TPEF	F: 5′-GCTGGAATTGCTCTGGTTATGATG-3′ R: 5′-CACAGGTGGATGTCTCCTTTTGACT-3′	60 (35)	330
COL1A2	F: 5′-CCCAGTGGTGAAGAAGGAAAGAGA-3′ R: 5′-GCATGACCTTTATCACCGTTTTTG-3′	60 (35)	419
ChIP			
C2TA-PIV region 1	F: 5′-GCCTGAAAAGGGAAAGTGACCACCTC-3′ R: 5′-CACACCCCCAGCCGTGGCAA-3′	60 (35)	111
C2TA-PIV region 2	F: 5′-ACAAGCTCCCTGCAACTCAG-3′ R: 5′-CCACCACGTGCTTTATCAGA-3′	64 (3), 62 (4), 60 (5), 58 (26)	187
C2TA-PIV region 3	F: 5′-GGGCTGAGAATCGAGGCTCCGAGAC-3′ R: 5′-GCGGGGATGCTGGAAACGAGGTG-3′	60 (35)	127
C2TA-PIV region 4	F: 5′-TCCTGCAGAGGTGCGCGCCCTTC-3′ R: 5′-CCGCCTGGAGAGCCCAATACCCAAGA-3′	60 (35)	134

Y = C or T, R = G or A

Immobilon-P membranes (Millipore). After blocking with 5% nonfat milk and 0.1% Tween-20 in Tris-buffered saline, membranes were incubated with anti-STAT1 rabbit polyclonal antibody (Cell Signaling, Beverly, MA, USA). The blots were visualized using enhanced chemiluminescence (Amersham).

Flow cytometry analysis

After treating the cell lines with 100 U/ml IFN-γ for 48 h, they were incubated first with fluorescein isothiocyanate (FITC)-conjugated anti-HLA-DR antibody (L243, ATCC), washed, and then incubated with affinity-purified, fluorescein-labeled goat anti-mouse IgG + IgM secondary antibody (Kirkegaard & Perry Laboratories, Gaithersburg, MD, USA). Groups of about 30 000 stained cells were then subjected to FACScan flow cytometry (Becton Dickinson Biosciences, Braintree, MA, USA), and the data obtained were analysed using CellQuest software (Becton Dickinson Biosciences).

Plasmids and transfection

The expression vector pIRES-CIITAPIV, which was constructed from HACIITA-PIV as previously described (Takamura *et al*., 2004), was kindly provided by Dr Jeremy M Boss of Emory University School of Medicine. The RKO colorectal cancer cell line was first cultured in Dulbecco's medium supplemented with 10% FBS. Cells (1×10^6) were transfected with either pIRESouro (Clontech Laboratories, Palo Alto, CA, USA) or pIRES-CIITAPIV by electroporation using Nucleofactor according to the manufacturer's instructions (Amaxa, Germany). Briefly, 2×10^6 cells were resuspended in 100 μl of Nucleofactor solution V (Amaxa) and then mixed with 3 μg of vector DNA. After transfection, the cells were plated and cultured in DMEM supplemented with 10% FBS and 0.5 μg/ml puromycin. After 2 weeks of selection, immunofluorescent staining for HLA-DR was carried out (see below).

Immunohistochemical staining

Cells were fixed in 3.7% formalin solution for 10 min at 25°C, washed with PBS, and incubated with rabbit anti-human HLA-DR (MBL, Nagoya, Japan) overnight. Immunofluorescent staining for phosphorylated STAT1 was carried out using antiphospho-STAT1 antibody (Cell Signalling) and Alexa 488 anti-mouse IgG (Cosmo Bio, Tokyo Japan), which served as the secondary antibody. Finally, the nucleus was stained with Vectashield mounting medium with DAPI (Vector Laboratories, Inc, Burlingame, CA, USA), and the cells were examined under a fluorescence microscope (Olympus, Tokyo, Japan). For immunohistochemical analysis of primary tumors, sections were dewaxed with xylene, and then incubated in a 100–50% ethanol series. The tumors were then divided into three groups according to the observed percentage of HLA-DR-positive tumor epithelium: 0–5, 5–50 and > 50%, respectively. Samples with 0–5% positive cells were considered negative, whereas samples with 5–50% positive cells were classified as weakly HLA-DR-positive, and those > 50% as strongly HLA-DR-positive.

Chromatin immunoprecipitation analysis (ChIP)

ChIP was carried out as described previously (Magdinier and Wolffe, 2001). Briefly, cells were harvested, and the proteins were cross-linked to DNA by adding formaldehyde to a final concentration of 1.0% for 10 min at 37°C. After allowing the fixed cells to settle on ice for 10 min, they were spun down by brief centrifugation, and the supernatant was carefully aspirated. The cells were then washed with ice-cold PBS containing protease inhibitors and resuspended in lysis buffer (1% SDS, 10 mM EDTA, 50 mM Tris-HCl, pH 8.0, and protease inhibitor). Nucleoprotein complexes were sonicated to reduce the DNA to fragments ranging from 200 to 1000 bp in size, after which immunoprecipitation was carried out for 16 h at 4°C with rotation, using anti-acetylated histone H3 antibody (Upstate Biotechnologies, Lake Placid, NY, USA) and anti-dimethylated histone H3K9 (Nakagawachi *et al*., 2003) as probes. The resultant immune complexes were collected using protein A-agarose beads, after which the DNA was purified by phenol/chloroform extraction, precipitated with ethanol and resuspended in water. About 1/100 of the precipitated DNA was used for PCR; 1/100 of the solution before adding antibody was used as an internal control for the amount of DNA. PCR was carried out in solution containing 1 × PCR buffer (TaKaRa), 1 μM primers, 0.25 mM dNTP mixture and 1.0 U of Hot Start *Taq* polymerase (TaKaRa). The primer sequences for the PCR reaction are shown in Table 2. The amplified products were subjected to agarose gel electrophoresis, and the intensity of resultant bands was calculated using a Lane and Spot Analyser (Atto, Japan).

Acknowledgements
We thank Dr William F Goldman for editing the manuscript. This study was supported in part by Grants-in-Aid for Scientific Research on Priority Areas from the Ministry of Education, Culture, Sports, Science, and Technology (MT, TT and KI). AS is a research fellow from the Japanese Society for the Promotion of Science. MT is a scholar supported by Research Grant of the Princess Takamatsu Cancer Research Fund.

References

Abril E, Real LM, Serrano A, Jimenez P, Garcia A, Canton J, Trigo I, Garrido F and Ruiz-Cabello F. (1998). *Cancer Immunol. Immunother.*, **47**, 113–120.
Andersen SN, Rognum TO, Lund E, Meling GI and Hauge S. (1993). *Br. J. Cancer*, **68**, 80–85.
Armstrong TD, Clements VK, Martin BK, Ting JP and Ostrand-Rosenberg S. (1997). *Proc. Natl. Acad. Sci. USA*, **94**, 6886–6891.
Armstrong TD, Clements VK and Ostrand-Rosenberg S. (1998). *J. Immunol.*, **160**, 661–666.
Baylin SB, Esteller M, Rountree MR, Bachman KE, Schuebel K and Herman JG. (2001). *Hum. Mol. Genet.*, **10**, 687–692.
Clark SJ, Harrison J, Paul CL and Frommer M. (1994). *Nucleic Acids Res.*, **22**, 2990–2997.
Croce M, De Ambrosis A, Corrias MV, Pistoia V, Occhino M, Meazza R, Giron-Michel J, Azzarone B, Accolla RS and Ferrini S. (2003). *Oncogene*, **22**, 7848–7857.
Fahrner JA, Eguchi S, Herman JG and Baylin SB. (2002). *Cancer Res.*, **62**, 7213–7218.
Garrido F and Algarra I. (2001). *Adv. Cancer Res.*, **83**, 117–158.
Jones PA and Baylin SB. (2002). *Nat. Rev. Genet.*, **3**, 415–428.
Kaklamanis L and Hill A. (1992). *Cancer Surv.*, **13**, 155–171.

Kanaseki T, Ikeda H, Takamura Y, Toyota M, Hirohashi Y, Tokino T, Himi T and Sato N. (2003). *J. Immunol.*, **170**, 4980–4985.

Kondo Y, Shen L and Issa JP. (2003). *Mol. Cell Biol.*, **23**, 206–215.

Landis SH, Murray T, Bolden S and Wingo PA. (1999). *CA Cancer J. Clin.*, **49**, 8–31, 1.

Lennon AM, Ottone C, Rigaud G, Deaven LL, Longmire J, Fellous M, Bono R and Alcaide-Loridan C. (1997). *Immunogenetics*, **45**, 266–273.

Liang G, Robertson KD, Talmadge C, Sumegi J and Jones PA. (2000). *Cancer Res.*, **60**, 4907–4912.

Lovig T, Andersen SN, Thorstensen L, Diep CB, Meling GI, Lothe RA and Rognum TO. (2002). *Br. J. Cancer*, **87**, 756–762.

Magdinier F and Wolffe AP. (2001). *Proc. Natl. Acad. Sci. USA*, **98**, 4990–4995.

McDougall CJ, Ngoi SS, Goldman IS, Godwin T, Felix J, DeCosse JJ and Rigas B. (1990). *Cancer Res.*, **50**, 8023–8027.

Meazza R, Comes A, Orengo AM, Ferrini S and Accolla RS. (2003). *Eur. J. Immunol.*, **33**, 1183–1192.

Morris AC, Spangler WE and Boss JM. (2000). *J. Immunol.*, **164**, 4143–4149.

Muhlethaler-Mottet A, Otten LA, Steimle V and Mach B. (1997). *EMBO J.*, **16**, 2851–2860.

Nakagawachi T, Soejima H, Urano T, Zhao W, Higashimoto K, Satoh Y, Matsukura S, Kudo S, Kitajima Y, Harada H, Furukawa K, Matsuzaki H, Emi M, Nakabeppu Y, Miyazaki K, Sekiguchi M and Mukai T. (2003). *Oncogene*, **22**, 8835–8844.

Neugut AI, Hayek M and Howe G. (1996). *Semin. Oncol.*, **23**, 281–291.

Nguyen CT, Weisenberger DJ, Velicescu M, Gonzales FA, Lin JC, Liang G and Jones PA. (2002). *Cancer Res.*, **62**, 6456–6461.

Ossendorp F, Toes RE, Offringa R, van der Burg SH and Melief CJ. (2000). *Immunol. Lett.*, **74**, 75–79.

Rhee I, Bachman KE, Park BH, Jair KW, Yen RW, Schuebel KE, Cui H, Feinberg AP, Lengauer C, Kinzler KW, Baylin SB and Vogelstein B. (2002). *Nature*, **416**, 552–556.

Rhee I, Jair KW, Yen RW, Lengauer C, Herman JG, Kinzler KW, Vogelstein B, Baylin SB and Schuebel KE. (2000). *Nature*, **404**, 1003–1007.

Santini V, Kantarjian HM and Issa JP. (2001). *Ann. Intern. Med.*, **134**, 573–586.

Sengupta PK, Smith EM, Kim K, Murnane MJ and Smith BD. (2003). *Cancer Res.*, **63**, 1789–1797.

Suzuki H, Itoh F, Toyota M, Kikuchi T, Kakiuchi H and Imai K. (2000). *Cancer Res.*, **60**, 4353–4357.

Takamura Y, Ikeda H, Kanaseki T, Toyota M, Tokino T, Imai K, Houkin K and Sato N. (2004). *Glia*, **45**, 392–405.

Ting JP and Trowsdale J. (2002). *Cell*, **109** (Suppl), S21–S33.

Toes RE, Ossendorp F, Offringa R and Melief CJ. (1999). *J. Exp. Med.*, **189**, 753–756.

Toyota M, Sasaki Y, Satoh A, Ogi K, Kikuchi T, Suzuki H, Mita H, Tanaka N, Itoh F, Issa JP, Jair KW, Schuebel KE, Imai K and Tokino T. (2003). *Proc. Natl. Acad. Sci. USA*, **100**, 7818–7823.

van den Elsen PJ, Gobin SJ, van der Stoep N, Datema G and Vietor HE. (2001). *J. Reprod. Immunol.*, **52**, 129–145.

Waldburger JM, Suter T, Fontana A, Acha-Orbea H and Reith W. (2001). *J. Exp. Med.*, **194**, 393–406.

Xiong Z and Laird PW. (1997). *Nucleic Acids Res.*, **25**, 2532–2534.

Yazawa T, Ito T, Kamma H, Suzuki T, Okudela K, Hayashi H, Horiguchi H, Ogata T, Mitsui H, Ikeda M and Kitamura H. (2002). *Am. J. Pathol.*, **161**, 291–300.

A dioxin sensitive gene, mammalian *WAPL*, is implicated in spermatogenesis

Masahiko Kuroda[a,b,c,*], Kosuke Oikawa[a,b,c], Tetsuya Ohbayashi[a,b,c,1], Keiichi Yoshida[a,c], Kazuhiko Yamada[d], Junsei Mimura[e], Yoichi Matsuda[d], Yoshiaki Fujii-Kuriyama[e], Kiyoshi Mukai[a]

[a] *Department of Pathology, Tokyo Medical University, 6-1-1 Shinjuku, Shinjuku-ku, Tokyo 160-8402, Japan*
[b] *CREST Research Project, Japan Science and Technology Corporation, 4-1-6 Kawaguchi, Saitama 332-0012, Japan*
[c] *Shinanomachi Research Park, Keio University, 35 Shinanomachi, Shinjuku-ku, Tokyo 160-8582, Japan*
[d] *Chromosome Research Unit, Faculty of Science, Hokkaido University, North 10 West 8, Kita-ku, Sapporo 060-0810, Japan*
[e] *Center for Tsukuba Advanced Research Alliance, University of Tsukuba, 1-1-1 Tenno-dai, Tsukuba, Ibaraki 305- 8577, Japan*

Received 26 October 2004; accepted 13 November 2004

Available online 2 December 2004

Edited by Lukas Huber

Abstract 2,3,7,8-Tetrachlorodibenzo-*p*-dioxin (TCDD) is an endocrine disruptor that produces a variety of toxic effects. We have isolated a mouse homolog of the *hWAPL* gene, termed *mouse WAPL* (*mWAPL*), as a target of TCDD by cDNA representational difference analysis from mouse embryonic stem cells. A statistically significant increase in *mWAPL* expression was observed at 0.1 μM TCDD in $AhR^{-/-}$ mouse embryonic fibroblast cells. Interestingly, at 1 μM TCDD, *mWAPL* mRNA levels decreased in $AhR^{+/+}$ cells, but further increased in $AhR^{-/-}$ cells. *hWAPL* and mWAPL were highly expressed only in testes among normal tissue samples, and we observed mWAPL localization in the synaptonemal complex of testicular chromosomes. In addition, mouse testes decreased the expression of *mWAPL* mRNA after a single intraperitoneal injection of TCDD. Thus, mammalian *WAPL* such as *hWAPL* and *mWAPL* may be involved in spermatogenesis and be target genes mediating the reproductive toxicity induced by TCDD.

Keywords: WAPL; 2,3,7,8-Tetrachlorodibenzo-*p*-dioxin; Spermatogenesis; Synaptonemal complex

1. Introduction

In *Drosophila melanogaster*, the protein encoded by the *wings apart-like* (*wapl*) gene regulates heterochromatin structure [1]. The *wapl* product is required to hold the sister chromatids of meiotic heterochromatin together. In addition, wapl is implicated in both heterochromatin pairing during female meiosis and the modulation of position-effect variegation (PEV). Moreover, a *P*-element screen of *Drosophila* identified wapl as a modifier of chromosome inheritance [2]. Recently, we have identified a novel human gene *hWAPL* that is a homolog of *wapl* [3]. *hWAPL* is overexpressed in invasive human cervical cancers and is often associated with cervical carcinogenesis. However, the essential function of hWAPL in normal cells is still unknown.

Dioxins, classified as endocrine disruptors, are ubiquitous in the environment. 2,3,7,8-tetrachlorodibenzo-*p*-dioxin (TCDD) is the most toxic dioxin and causes a variety of effects, including immunotoxicity, hepatotoxicity, teratogenicity, and tumor promotion [4,5]. Changes in gene expression induced by TCDD and related chemicals are initiated by the binding of the compounds to the aryl hydrocarbon receptor (AhR). AhR then dimerizes with the aryl hydrocarbon receptor nuclear translocator to form a complex that interacts with gene regulatory elements containing a xenobiotic response element (XRE) motif [6]. AhR mediates many of the TCDD-induced changes in gene expression. Many of the target genes responsible for the symptoms of toxicity, however, remain unidentified.

Previously, we performed a cDNA representational difference analysis (RDA) of the cDNA derived from mouse ES cells treated or not with TCDD in order to isolate genes induced by TCDD. This procedure identified three genes, temporarily termed *Dioxin Inducible Factor 1*, *2*, and *3* (*DIF-1*, *DIF-2*, and *DIF-3*), that were induced in TCDD-treated ES cells. *DIF-1* is identical to the gene encoding histamine releasing factor (HRF) [7] and *DIF-3* is the gene encoding a novel protein with a C2H2 zinc-finger domain [8]. However, *DIF-2* has not yet been characterized.

In this study, we have identified the gene corresponding to *DIF-2* as a mouse homolog of *wapl* and *hWAPL*, termed *mouse WAPL* (*mWAPL*). We have also confirmed the effects of TCDD on *mWAPL* expression and investigated the localization of mWAPL protein in normal adult mice to reveal the participation of mWAPL in TCDD-induced toxicity.

2. Materials and methods

2.1. cDNA cloning and sequencing

To isolate the complete mWAPL cDNA, we used total RNA from mouse testes. The full-length mWAPL cDNA was amplified by reverse transcription-PCR with primers designed from a computer search. We determined the nucleotide sequence of the cDNA with an Applied Biosystems 310 automated DNA sequencer.

*Corresponding author. Fax: +81 3 3352 6335.
E-mail address: kuroda@tokyo-med.ac.jp (M. Kuroda).

[1] Present address: Horizontal Medical Research Organization, Kyoto University Faculty of Medicine, Yoshida-Konoe-cho, Sakyo-ku, Kyoto, 606-8501, Japan.

Abbreviations: TCDD, 2,3,7,8-tetrachlorodibenzo-*p*-dioxin; AhR, aryl hydrocarbon receptor; MEF, mouse embryonic fibroblast

0014-5793/$22.00
doi:10.1016/j.febslet.2004.11.070

2.2. Cell cultures and chemicals

$AhR^{-/-}$ embryos were generated from intercrossed $AhR^{+/-}$ mice [9]. Mouse embryonic fibroblasts (MEFs) of wild-type or mutant genotypes were harvested from day 14.5 mouse embryos. MEFs were grown as previously described [10]. 2,3,7,8-Tetrachlorodibenzo-*p*-dioxin (TCDD) (Cambridge Isotope Laboratories, Inc., Andover, MA) was prepared in dimethylsulfoxide (DMSO).

2.3. RNA isolation, quantitative real time PCR, and Northern blot analysis

RNA isolation was performed as described [10]. First strand cDNA synthesis was performed as described [11]. Real time PCR analysis was performed using the Smart Cycler System (Cepheid, Sunnyvale, CA) with SYBR Green I (Cambrex, Washington, DC). Real time PCR utilized *mWAPL* specific primers, 5′-ACCTGGTGGAGTATAGTGCCC-3′ and 5′-TGGCAGAGACACCCAAGAAGC-3′; mouse *β-actin* specific primers, 5′-AGCCTTCCTTCTTGGGTATGG-3′ and 5′-CACTTGCGGTGCACGATGGAG-3′; or *CYP1A1* specific primers, 5′-TTTGGTTTGGGCAAGCGA-3′ and 5′-GTCTAAGCCTGAAGATGC-3′. Reaction mixtures were denatured at 95 °C for 30 s, then subjected to 40 PCR cycles at either 95 °C for 3 s, 68 °C for 30 s, and 86 °C for 6 s for *mWAPL*, or 95 °C for 3 s, 68 °C for 30 s, and 85 °C for 6 s for mouse *β-actin* and *CYP1A1*. mRNA levels of *mWAPL* and *CYP1A1* were determined by normalization of their signals to *β-actin* signals. We performed the experiments to evaluate mRNA levels in triplicate. The data were analyzed using Student's *t* test, and $Ps < 0.01$ were considered to indicate significant differences.

For Northern blot analysis, the 567-bp *Dpn*II fragment of *mWAPL* cDNA and a PCR-amplified mouse *β-actin* cDNA fragment using the primers described above were used as probes and labeled with ^{32}P using the Rediprime II random prime labeling system (Amersham Biosciences, Piscataway, NJ). To examine *hWAPL* expression in various human tissues, we used Human MTN Blot I, II and III (Clontech, #7760-1, #7759-1 and #7767-1, respectively).

2.4. Immunoblot analysis and Immunohistochemistry

To generate polyclonal antibodies against hWAPL, we immunized rabbit against a 6× histidine-tagged hWAPL COOH terminus (amino acids 814–1037) fusion protein and obtained an anti-hWAPL polyclonal antibody (480-02). The anti-hWAPL polyclonal antibody was used at the dilution of 1:2000 for Immunoblot analysis and Immunohistochemistry. Immunoblot analyses were performed as previously described [7]. Protein samples from adult mouse tissues were prepared in RIPA buffer [7] and quantified using the BioRad protein assay (Nippon Bio-Rad Laboratories, Tokyo, Japan). Immunohistochemical analysis was performed on formalin-fixed paraffin-embedded sections using Ventana HX System Benchmark (Ventana Medical Systems INC., Tucson, AZ). As a control of specificity, the anti-hWAPL polyclonal antibody (480-02) was pre-incubated for 18 h at 4 °C with a recombinant hWAPL protein and then applied to immunohistochemistry.

2.5. Immunocytology

The slides with surface-spread spermatocyte nuclei were prepared for immunocytological analysis as previously described [12]. Then, the anti-hWAPL polyclonal antibody (480-02) was diluted 1:400 and used as the primary antibody. After incubation with the primary antibody, the slide was reacted with goat anti-rabbit IgG conjugated to fluorescein isothiocyanate. DNA was visualized by counter-staining with 4′, 6-diamidine-2-phenylindole (DAPI).

2.6. Animals and treatment

Guidelines for the care and use of animals were approved by the animal research center at Tokyo Medical University. C57/BL6 male mice (13 weeks old) were purchased from Oriental Yeast Co., Ltd. (Tokyo, Japan). Each mouse received one intraperitoneal injection of 200 μl saline and 12.5 μl DMSO containing TCDD at a dose of 600 μg/kg of body mass. Control mice were injected with the same solution without TCDD. Testis samples were harvested 24 h after injection and subjected to real time PCR analysis.

3. Results and discussion

3.1. Molecular cloning of mouse WAPL

Using BLAST, we found that the nucleotide sequence of the DNA fragment corresponding to *Dioxin Inducible Factor-2* (*DIF-2*) is included in mKIAA0261, which is a mouse KIAA-homolog [13]. This suggested that *DIF-2* might be a homolog of the *hWAPL* gene because *hWAPL* corresponds to the KIAA0261 cDNA fragment [3]. Thus, we renamed the *DIF-2* gene *mouse WAPL* (*mWAPL*). Based on the mKIAA0261 sequence, we cloned and confirmed the nucleotide sequence of the full-length coding region of the cDNA for *mWAPL* (Database Accession No. AB167349). Multiple sequence alignment of the proteins encoded by *mWAPL*, *hWAPL*, and *wapl* demonstrated that the three proteins are similar not only in the WAPL conserved region [3], but throughout the entire protein (Fig. 1) (mWAPL is 92% identical and 96% similar to hWAPL, and 24% identical and 45% similar to wapl). Thus, the protein encoded by *mWAPL* may be involved in heterochromatin organization, PEV modification and chromosome inheritance like the wapl protein in *Drosophila*.

3.2. Effects of TCDD on MEFs

To confirm the effects of TCDD on *mWAPL* expression, we examined *mWAPL* mRNA levels in $AhR^{+/+}$ and $AhR^{-/-}$ MEFs treated with 0, 0.01, 0.1, and 1 μM TCDD for 2 h by Northern blot analysis. Although *mWAPL* signals were on the whole extremely weak and barely visualized by strong enhancement, we found that *mWAPL* mRNA levels in $AhR^{-/-}$ MEFs showed the highest at 1 μM TCDD; in $AhR^{+/+}$ MEFs, on the other hand, *mWAPL* mRNA level at 0.1 μM TCDD was maximum (Fig. 2A). The two hybridization signals observed for *mWAPL* are similar to those observed in Northern blots for *hWAPL* and, as previously discussed [3], may reflect the difference of the length of the untranslated regions of the *WAPL* mRNAs.

To evaluate the *mWAPL* mRNA levels more accurately, we performed quantitative real time PCR analysis and confirmed the expression pattern of *mWAPL* mRNA in $AhR^{+/+}$ and $AhR^{-/-}$ MEFs (Fig. 2B). We did not find significant differences of cell cycle profile of these MEF cells by flow cytometric analysis (data not shown). Thus, although further investigation is required, the *mWAPL* gene may be inducible by TCDD independent of the AhR-mediated pathway but downregulated by a direct target molecule of TCDD in the AhR-dependent pathway.

3.3. Expression of mammalian WAPL in testes

Our previous study showed that *hWAPL* is expressed only in uterine cervical cancer among human tumor and normal control tissue samples examined [3]. Here, we examined mWAPL expression in normal mouse tissues by Western blot analysis and detected strong expression of mWAPL protein in the testes (Fig. 3A). Therefore, we also investigated *hWAPL* expression in various normal human tissues by Northern blot analysis, and confirmed that *hWAPL* mRNA was expressed abundantly in the testes, with weak expression in all other normal human tissues (Fig. 3B). Two hybridization signals for *hWAPL* mRNAs were visible in testes similar to MEFs (Fig. 2A) and previously reported results in cervical cancer tissues [3].

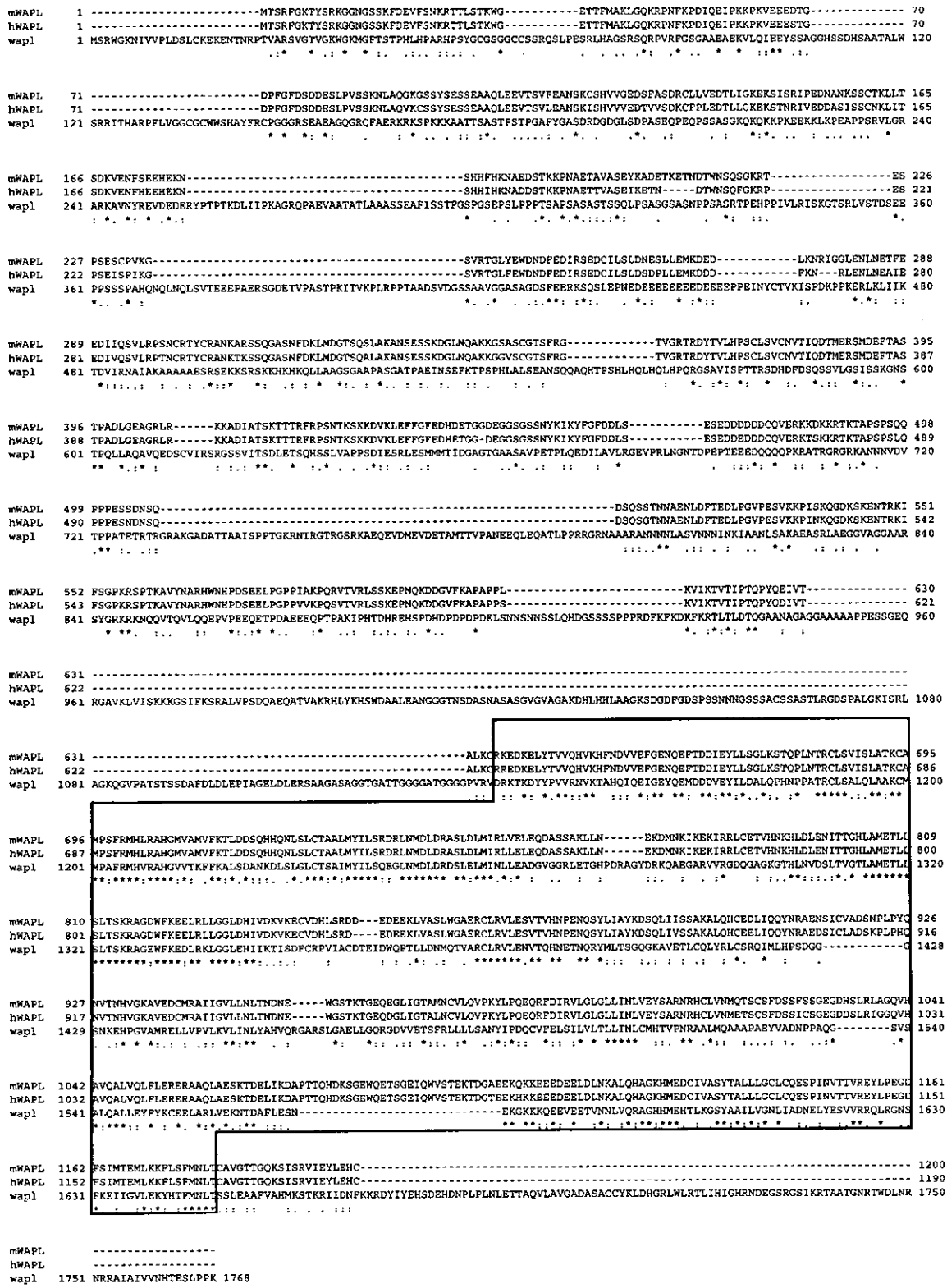

Fig. 1. Sequence alignment of WAPL homologs. The deduced amino acid sequences of mWAPL, hWAPL (Database Accession No. AB065003) and *Drosophila* wapl (Database Accession No. U40214) were aligned using CLUSTAL W multiple sequence alignment program. (*) indicates positions which have a single, fully conserved residue; (:) indicates that one of the following 'strong' groups is fully conserved: (STA), (NEQK), (NHQK), (NDEQ), (QHRK), (MILV), (MILF), (HY) and (FYW); and (·) indicates that one of the following 'weaker' groups is fully conserved: (CSA), (ATV), (SAG), (STNK), (STPA), (SGND), (SNDEQK), (NDEQHK), (NEQHRK), (FVLIM), and (HFY). The boxed region indicates the WAPL-conserved region.

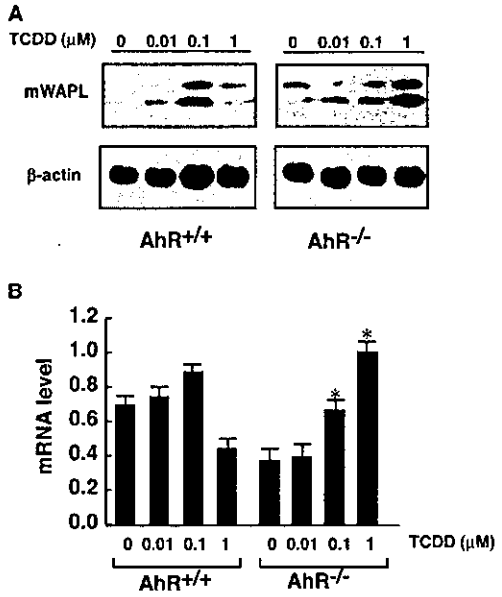

Fig. 2. Effects of TCDD on $AhR^{+/+}$ and $AhR^{-/-}$ MEFs. (A) Northern blot analysis of *mWAPL* in $AhR^{+/+}$ and $AhR^{-/-}$ MEFs treated with 0.1% DMSO and 0, 0.01, 0.1, or 1 μM TCDD for 2 h. The blots were hybridized with a probe for *mWAPL* (upper) and then reprobed with a *β-actin* probe as loading control (lower). (B) *mWAPL* mRNA levels in $AhR^{+/+}$ and $AhR^{-/-}$ MEFs treated with 0.1% DMSO and 0, 0.01, 0.1, or 1 μM TCDD for 2 h were determined with quantitative real time PCR analysis. The *mWAPL* mRNA levels were determined by normalization of *mWAPL* signals to *β-actin* signals, and the maximum mRNA expression level was arbitrarily set to 1 in the graphical presentation (*Y*-axis). The data were obtained from three independent experiments. Columns: means; bars: S.D. *, $P < 0.001$ versus the $AhR^{-/-}$ MEFs at 0 μM of TCDD.

We next examined the expression pattern of mWAPL in testes by immunohistochemical analysis using formalin-fixed mouse samples (Fig. 3C). The results showed that mWAPL was expressed abundantly in large pachytene spermatocytes, which are conspicuous for their size and loose organization of their chromatin, whereas it was undetectable in condensing forms of sperm (Fig. 3C, panel 2). We did not find any positive staining with the antibody after pre-absorption with a recombinant hWAPL protein (Fig. 3C, panel 3). These results suggested that mWAPL is expressed predominantly in early stages of spermatogenesis. similar results were observed in frozen sections (data not shown).

We have also characterized the subcellular localization of mWAPL in early spermatocytes by immunocytological staining. mWAPL immunoreactivity was detected at both zygotene (Fig. 3D) and pachytene stage (Fig. 3E). The antibody stained both unsynapsed and synapsed axial element components in early zygonema, and localized to the fully synapsed bivalents (synaptonemal complex) and the partially synapsed X and Y chromosomes (Fig. 3E, panel 3). From these results, hWAPL and mWAPL may be implicated in spermatogenesis. Although additional evidences are required, we suspect that mammalian WAPL may play a significant role in meiosis as does *Drosophila wapl* [1].

Furthermore, because of the localization of mWAPL in pachynema, we expect that mammalian WAPL functions in homologus recombination and DNA recombination. DNA double-strand breaks (DSB) constitute the most dangerous type of DNA damage induced by ionizing radiation.The gene

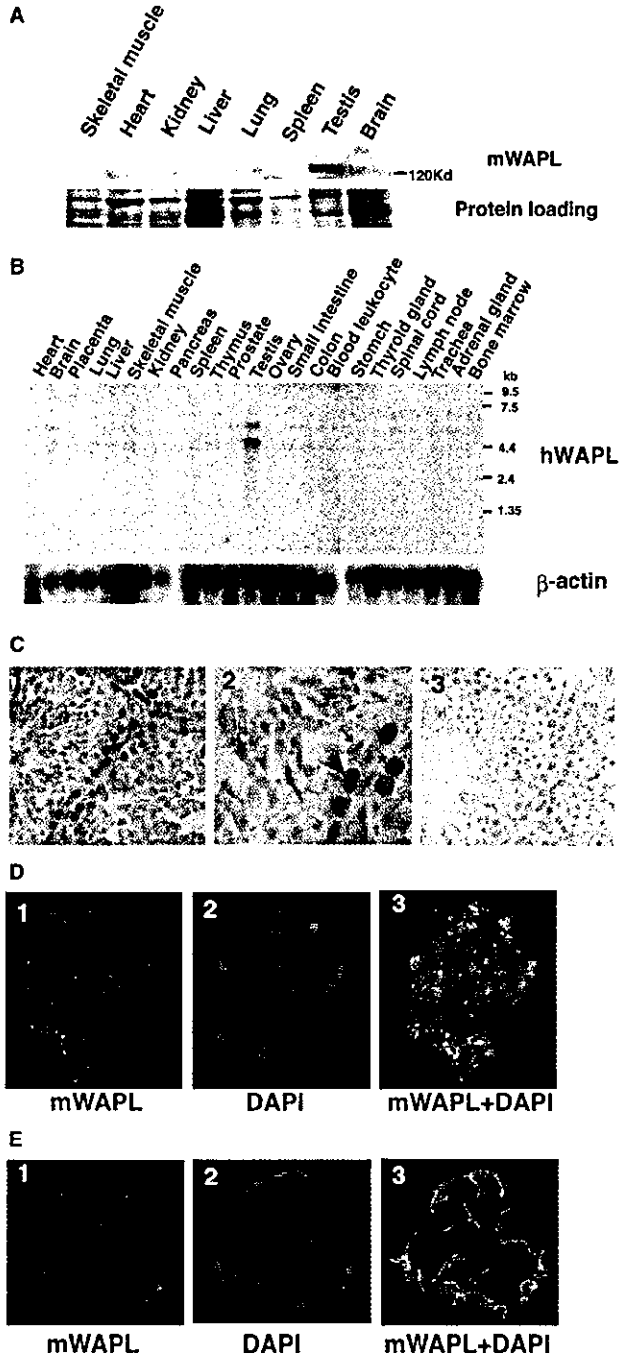

Fig. 3. Expression of mammalian WAPL in testes. (A) Western blot analysis of mWAPL in various normal mouse tissues. A Ponceau-stained nitrocellulose membrane is also shown as a control for protein loading (lower panel). (B) Northern blot analysis of *hWAPL* in various normal human tissues. *β-actin* signals are also shown as loading control. (C) mWAPL immunostaining in adult mouse testes. Formalin-fixed and paraffin-embedded 5 μm sections of mouse testes were treated with an anti-hWAPL antibody (panels 1 and 2), or the antibody after pre-absorption with a recombinant hWAPL protein as a negative control (panel 3), a horseradish peroxidase-conjugated secondary antibody, developed with diaminobenzidine, and counterstained with hematoxylin. Specific cell types in the seminiferous epithelium are identified in panel 2: arrowhead, pachytene spermatocyte; arrow, round spermatid; asterisk, Sertoli cell. (D) Chromosomal spread of spermatocyte at early zygotene fixed and stained with anti-hWAPL antibody and DAPI (panel 1, mWAPL; panel 2, DAPI; panel 3, mWAPL + DAPI). (E) Chromosomal spread of spermatocyte at mid pachytene fixed and stained for mWAPL and DAPI (panel 1, mWAPL; panel 2, DAPI; panel 3, mWAPL + DAPI).

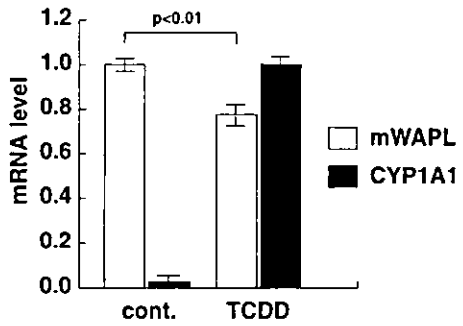

Fig. 4. Mouse testes exhibited a decreased level of mWAPL after TCDD treatment. *mWAPL* mRNA levels in testes of mice treated with or without TCDD (at a dose of 600 μg/kg of body mass) for 24 h were determined by quantitative real time PCR analysis. The data represent the means of eight samples. *CYP1A1* mRNA levels were also determined as a control for the effects of TCDD on testes. The *mWAPL* and *CYP1A1* mRNA levels were determined by normalization of their signals to *β-actin* signals, respectively, and the maximum mRNA expression level was arbitrarily set to 1 in the graphical presentation (*Y*-axis). Bars: S.E.

that is implicated in homologous recombination might work at DSB repair [14,15] and the alterations in recombination promote carcinogenesis by causing genomic instability. Therefore, unscheduled expression of mammalian WAPL by human papillomavirus (HPV) [16], TCDD or other agents may cause an inaccurately repaired or unrepaired DSB and result in mutations or genomic rearrangements in surviving cells, which in turn leads to genomic instability and subsequently results in malignant cell transformation or defects in embryogenesis.

Recently, we have characterized another dioxin inducible gene named *Dioxin Inducible Factor 3* (*DIF-3*) that is highly expressed in testes [8]. Interestingly, DIF-3 is expressed most strongly in the large pachytene spermatocytes [8] similar to mWAPL. However, we have not found any evidence of functional association between mWAPL and DIF-3 until now.

3.4. Downregulation of mWAPL expression by TCDD in testes

These results prompted us to examine whether the expression of mWAPL was influenced by TCDD in testes. Twenty hours after the injection of TCDD into the abdominal cavities of C57/BL6 mice, we harvested the testes and analyzed *mWAPL* expression by quantitative real time PCR analysis. Because the *CYP1A1* gene is a well-known target of TCDD, we also calculated *CYP1A1* mRNA levels to confirm the effects of TCDD on testes. The mice exhibited a decrease in *mWAPL* expression and a marked increase in *CYP1A1* expression compared to control mice (Fig. 4). This result suggests that TCDD exposure affects mWAPL expression levels in testes.

In recent years, several reports have focused on certain man-made toxins known as endocrine disrupting chemicals (EDCs) that persist in the environment. These chemicals are capable of altering the endocrine homeostasis of an animal, thereby causing serious reproductive and developmental defects as well as testicular oncogenesis [17–19]. Several studies have also provided evidence of a decline in semen quality and/or sperm counts over the same period [19]. Our previous study demonstrated that hWAPL overexpression induces carcinogenesis and tumor progression, and that hWAPL reduction by small interfering RNA (siRNA) induces cell death [3]. These observations suggest that unscheduled changes in hWAPL expression can cause severe damage to cells. Thus, although more experiments are needed to provide direct evidence linking mammalian *WAPL* with TCDD-induced reproductive toxicity, the present study suggests that mammalian *WAPL* may be a target gene mediating the reproductive toxicity of TCDD.

Acknowledgments: We thank E. Aoki, Y. Matsunaga, H. Sanai, S. Tsukamoto, and T. Hanashi for their expert technical assistance. This work was supported by a Grant-in-Aid for Scientific Research on Priority Area (C) (to M.K.) and a Grant-in-Aid for Encouragement of Young Scientists (to M.K.) from the Ministry of Education, Science, Sports and Culture, and Core Research for Evolutional Science and Technology (CREST) (to M.K.) from Japan Science and Technology Corporation.

References

[1] Verni, F., Gandhi, R., Goldberg, M.L. and Gatti, M. (2000) Genetic and molecular analysis of wings apart-like (wapl), a gene controlling heterochromatin organization in *Drosophila melanogaster*. Genetics 154, 1693–1710.
[2] Dobie, K.W., Kennedy, C.D., Velasco, V.M., McGrath, T.L., Weko, J., Patterson, R.W. and Karpen, G.H. (2001) Identification of chromosome inheritance modifiers in *Drosophila melanogaster*. Genetics 157, 1623–1637.
[3] Oikawa, K., Ohbayashi, T., Kiyono, T., Nishi, H., Isaka, K., Umezawa, A., Kuroda, M. and Mukai, K. (2004) Expression of a novel human gene, human wings apart-like (hWAPL), is associated with cervical carcinogenesis and tumor progression. Cancer Res. 64, 3545–3549.
[4] Chapman, D.E. and Schiller, C.M. (1985) Dose-related effects of 2,3,7,8-tetrachlorodibenzo-*p*-dioxin (TCDD) in C57BL/6J and DBA/2J mice. Toxicol. Appl. Pharmacol. 78, 147–157.
[5] McGregor, D.B., Partensky, C., Wilbourn, J. and Rice, J.M. (1998) An IARC evaluation of polychlorinated dibenzo-*p*-dioxins and polychlorinated dibenzofurans as risk factors in human carcinogenesis. Environ. Health Perspect. 106 (Suppl. 2), 755–760.
[6] Sogawa, K. and Fujii-Kuriyama, Y. (1997) Ah receptor, a novel ligand-activated transcription factor. J. Biochem. (Tokyo) 122, 1075–1079.
[7] Oikawa, K., Ohbayashi, T., Mimura, J., Fujii-Kuriyama, Y., Teshima, S., Rokutan, K., Mukai, K. and Kuroda, M. (2002) Dioxin stimulates synthesis and secretion of IgE-dependent histamine-releasing factor. Biochem. Biophys. Res. Commun. 290, 984–987.
[8] Ohbayashi, T., et al. (2001) Dioxin induces a novel nuclear factor, DIF-3, that is implicated in spermatogenesis. FEBS Lett. 508, 341–344.
[9] Mimura, J., et al. (1997) Loss of teratogenic response to 2,3,7,8-tetrachlorodibenzo-*p*-dioxin (TCDD) in mice lacking the Ah (dioxin) receptor. Genes Cells 2, 645–654.
[10] Oikawa, K., et al. (2001) Dioxin suppresses the checkpoint protein, MAD2, by an aryl hydrocarbon receptor-independent pathway. Cancer Res. 61, 5707–5709.
[11] Kuroda, M., Ishida, T., Takanashi, M., Satoh, M., Machinami, R. and Watanabe, T. (1997) Oncogenic transformation and inhibition of adipocytic conversion of preadipocytes by TLS/FUS-CHOP type II chimeric protein. Am. J. Pathol. 151, 735–744.
[12] Matsuda, Y., Moens, P.B. and Chapman, V.M. (1992) Deficiency of X and Y chromosomal pairing at meiotic prophase in spermatocytes of sterile interspecific hybrids between laboratory mice (*Mus domesticus*) and *Mus spretus*. Chromosoma 101, 483–492.
[13] Okazaki, N., et al. (2003) Prediction of the coding sequences of mouse homologues of KIAA gene: III. the complete nucleotide sequences of 500 mouse KIAA-homologous cDNAs identified

by screening of terminal sequences of cDNA clones randomly sampled from size-fractionated libraries. DNA Res. 10, 167–180.
[14] Kuroda, M., et al. (2000) Male sterility and enhanced radiation sensitivity in TLS(−/−) mice. EMBO J. 19, 453–462.
[15] Willers, H., Dahm-Daphi, J. and Powell, S.N. (2004) Repair of radiation damage to DNA. Br. J. Cancer 90, 1279–1301.
[16] Kuroda, M., Kiyono, T., Oikawa, K., Yoshida, K. and Mukai, K. Br. J Cancer (in press).
[17] Birnbaum, L.S. (1995) Developmental effects of dioxins and related endocrine disrupting chemicals. Toxicol. Lett. 82–83, 743–750.
[18] Brouwer, A., et al. (1995) Functional aspects of developmental toxicity of polyhalogenated aromatic hydrocarbons in experimental animals and human infant. Eur. J. Pharmacol. 293, 1–40.
[19] Sharpe, R.M. and Skakkebaek, N.E. (1993) Are oestrogens involved in falling sperm counts and disorders of the male reproductive tract?. Lancet 341, 1392–1395.

British Journal of Cancer (2005) 92, 290–293

www.bjcancer.com

Short Communication

The human papillomavirus E6 and E7 inducible oncogene, *hWAPL*, exhibits potential as a therapeutic target

M Kuroda[*,1,2,3,5], T Kiyono[4,5], K Oikawa[1,2,3,5], K Yoshida[1,3] and K Mukai[1]

[1]Department of Pathology, Tokyo Medical University, Shinjuku-ku, Tokyo 160-8402, Japan; [2]CREST Research Project, Japan Science and Technology Corporation, Kawaguchi-shi, Saitama 332-0012, Japan; [3]Shinanomachi Research Park, Keio University, Shinjuku-ku, Tokyo 160-8582, Japan; [4]Division of Virology, National Cancer Center Research Institute, Chuo-ku, Tokyo 104-0045, Japan

Here we show that human papillomavirus (HPV) E6 and E7 oncoproteins induce hWAPL expression. In addition, small interfering RNA (siRNA) of *hWAPL* suppressed the growth of tumours derived from SiHa cells in nude mice. Thus, hWAPL may be one of the effective targets of uterine cervical cancer therapy.
British Journal of Cancer (2005) **92,** 290–293. doi:10.1038/sj.bjc.6602329 www.bjcancer.com
Published online 11 January 2005

Keywords: hWAPL; HPV; E6; E7; siRNA

Cervical cancer is unique due to its association with high-risk human papilloma virus (HPV) infection with strains such as HPV-16 and HPV-18 (zur Hausen, 1996). The high-risk-HPV oncoproteins, E6 and E7, are necessary for immortalisation and transformation of cervical keratinocytes (Munger *et al*, 1989). E6 binds to the wild-type p53 protein and promotes its ubiquitin-dependent degradation (Scheffner *et al*, 1990, 1993), and E7 binds to the retinoblastoma protein Rb and disrupts the complex between Rb and the E2F transcription factor family, which controls the expression of genes involved in cell-cycle progression (Dyson *et al*, 1992). Therefore, the development of anticancer therapies that target HPV E6 and E7 and/or downstream targets of HPV E6 and E7 might be a specific and effective treatment for cervical cancer. In fact, RNA interference (RNAi) of E6 and/or E7 inhibits growth of HPV-positive cancer cells (Jiang and Milner, 2002; Butz *et al*, 2003; Yoshinouchi *et al*, 2003).

Our previous study demonstrated that the novel human gene *hWAPL* showed the unscheduled high-level expression in cervical dysplasia and carcinoma (Oikawa *et al*, 2004). In addition, NIH3T3 cells overexpressing hWAPL developed into tumours upon injection into nude mice, suggesting that hWAPL plays a significant role in cervical carcinogenesis and tumour progression as an oncogene (Oikawa *et al*, 2004). Furthermore, siRNA of *hWAPL* inhibited cell growth in cervical cancer-derived cultured cells (Oikawa *et al*, 2004).

In this report, we reveal that HPV E6 and E7 oncoproteins affect hWAPL expression. We also show that hWAPL exhibited great potential as a novel therapeutic target molecule in the treatment of cervical cancer.

*Correspondence: Dr M Kuroda, Department of Pathology, Tokyo Medical University, 6-1-1, Shinjuku, Shinjuku-ku, Tokyo 160-8402, Japan; E-mail: kuroda@tokyo-med.ac.jp
[5] These authors contributed equally
Received 31 August 2004; revised 12 October 2004; accepted 15 October 2004; published online 11 January 2005

MATERIALS AND METHODS

Cell culture, retroviral vector construction and retroviral infection

SiHa, CaSki and C33A cells were grown in DMEM (Sigma Chemical Co., St Louis, MO, USA) containing 10% fetal bovine serum (FBS) at 37°C in a 5% CO_2 environment. Normal human epidermal keratinocytes from adult skin (HDK1) were grown in keratinocyte serum-free medium (K-SFM; Invitrogen, Carlsbad, CA, USA).

The HPV16-E6, E7, and E6E7 genes were amplified by polymerase chain reaction (PCR) using the following primers: 5′-AAAAAGCAGGCTCCACCATGTTTCAGGACCCACAGGAGCGACCC-3′ and 5′-AGAAAGCTGGGTTACAGCTGGGTTTCTCTACGTG-3′ for E6, and 5′-AAAAAGCAGGCTCCACCATGCATGGAGATACACCTACAT-3′ and 5′-AGAAAGCTGGGTTATGGTTTCTGAGAACAGATGGGG-3′ for E7. The amplified DNA fragments were cloned into the retroviral vector, pCLXSN.

The bovine papillomavirus type 1 (BPV1) E2 segment was obtained by nested PCR from a pBPV-MII template using 5′-GGGGACAAGTTTGTACAAAAAAGCAGGCT-3′ and 5′-GGGGACCACTTTGTACAAGAAAGCTGGGT-3′ as outer primers, and 5′-AAAAAGCAGGCTCCACCATGGAGACAGCATGCGAAC-3′ and 5′-AGAAAGCTGGGTCAGAAGTCCAAGCTGGCTGTAAAG-3′ as inner primers. The BPV1 E2 segment was then cloned into a pCMSCV-based (Clontech, Palo Alto, CA, USA) retroviral vector, pCMSVpuro.

The preparation of recombinant retroviruses and the infection procedures have been previously described (Naviaux *et al*, 1996). HDK1 cells were infected with the prepared retroviruses, LXSN-16E6, LXSN-16E7, LXSN-16E6E7, or the control LXSN. The infected cells were selected in the presence of 50 $\mu g\,ml^{-1}$ of G418. SiHa, CaSki and C33A cells were infected with either the MSCV-puro or MSCV-puroBPV1E2 viruses and selected with 1 $\mu g\,ml^{-1}$ of puromycin.

Immunoblot analysis

We generated a rabbit polyclonal antibody against a synthetic peptide, amino acids 50–66 (CNFKPDIQEIPKKPKVEE) of hWAPL

(termed anti-hWAPL-N). Immunoblot analyses were performed as previously described (Kiyono *et al*, 1997). Antibodies against hWAPL (anti-hWAPL-N), p53 (Oncogene Science, Cambridge, MA, USA, DO-1), and the anti-HPV16 E7 (ZYMED, South San Francisco, CA, USA, 8C9) were used at a dilution of 1/1000.

Animals and treatments

Guidelines for the care and use of animals were approved by the animal research centre in Tokyo Medical University. BALB/cAJcl-nu female mice (4 weeks old) were purchased from Charles River Japan, Inc. (Kanagawa, Japan). The individual mice were injected with $\approx 4 \times 10^7$ SiHa cells suspended in 200 μl of PBS. Upon the development of a tumour from the injected SiHa cells 1 week after injection, we injected either an active siRNA specific for *hWAPL* or the negative control siRNA at the indicated time points (Figures 2A and 3). The nucleotide sequences of the siRNAs were as previously described (Oikawa *et al*, 2004). The active siRNA specific for *hWAPL* corresponds to siRNA(I) in the previous study (Oikawa *et al*, 2004). The injection materials were generated as follows: In Figure 2, the siRNAs were synthesised by *in vitro* transcription using a Silencer siRNA Construction Kit (Ambion, Austin, TX, USA). One microlitre of 10 μM siRNA and 2 μl of Oligofectamine Reagent (Invitrogen Japan, Tokyo, Japan) were diluted into 89 μl and 8 μl of Opti-MEM I (Invitrogen Japan), respectively. After a 10-min incubation, the diluted reagents were combined and incubated for an additional 20 min. The siRNA-Oligofectamine mixture was then injected into the mouse at the tumour site. In Figure 3, 1 μl of 10 μM siRNA and 74 μl of 2% atelocollagen (Koken Co. Ltd, Tokyo, Japan) (Takei *et al*, 2004) were mixed on ice, and then the siRNA-atelocollagen mixture was injected into mouse at the tumour site.

Statistical analysis

The data were analysed using the Student's *t*-test, and $P < 0.001$ were considered to indicate significant differences.

RESULTS

HPV oncoproteins E6 and E7 induce hWAPL

We examined whether HPV-16 E6 and E7 oncogene products influence hWAPL expression. We infected normal human epidermal keratinocytes from adult skin tissue (HDK1) with HPV-16 E6- and E7-expressing retroviruses, and observed that both HPV-16 E6 and E7 induce hWAPL expression (Figure 1A). E6 and E7 expression levels were confirmed by monitoring p53 degradation and E7 antibody staining, respectively (Figure 1A).

To confirm that hWAPL expression is inducible by E6 and E7, we also examined whether repression of E6 and E7 expression causes hWAPL reduction in cervical cancer-derived cell lines. Because the papillomavirus E2 protein represses E6/E7 transcription by binding the HPV early promoter (Hwang *et al*, 1993, 1996; Dowhanick *et al*, 1995; Francis *et al*, 2000), we analyse the effect of E2 on hWAPL expression. We observed a significant reduction of hWAPL protein levels after the infection of HPV-16 E6- and E7-expressing cervical cancer cell lines, such as CaSki and SiHa, with the retrovirus encoding E2 (Figure 1B). The HPV-negative cervical cancer cell line C33A, however, did not exhibit significant changes in hWAPL protein levels after E2 retrovirus infection (Figure 1B). These results demonstrate that hWAPL can be induced by HPV E6 and E7 oncoproteins.

The mechanism of hWAPL induction by E6 and E7 has not yet been elucidated. Although both E6 and E7 contribute transformation of human keratinocytes, functions of these proteins are different. hWAPL induction by the combination of E6 and E7, however, showed similar level to that by either E6 or E7 alone (Figure 1A). Thus, *hWAPL* transcription may possibly respond to a particular precancerous cell states induced by E6 and/or E7. In fact, HPV-positive normal cervical tissue samples exhibited a low level of hWAPL expression (Oikawa *et al*, 2004), and C33A, an HPV-negative uterine cervical cancer-derived cell line, showed high hWAPL expression (Figure 1B, and data not shown), suggesting that hWAPL expression is more closely related with cervical carcinogenesis than HPV infection, as previously mentioned (Oikawa *et al*, 2004). Nevertheless, although HPV infection does not always induce hWAPL expression, E6 and E7 oncoproteins are still likely to be associated with hWAPL expression in cervical cancers.

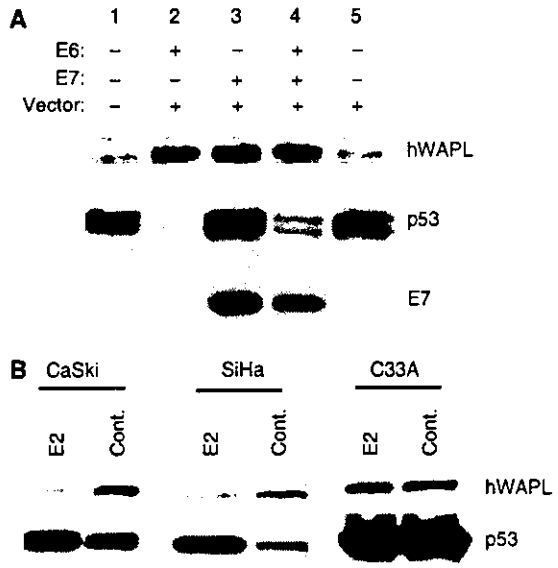

Figure 1 (**A**) HPV-16 E6 and E7 expression induces increased expression of hWAPL. hWAPL protein was induced by HPV E6 and E7 oncoprotein expression in HDK1 cells (passage 5), as determined by Western blotting. E6 induced p53 degradation (lanes 2, E6 and 4, E6E7). A Western blot showing HPV-16 E7 protein levels is provided in the bottom panel. (**B**) BPV1 E2 suppressed hWAPL expression. hWAPL protein levels were reduced by exogenous BPV1 E2 expression in the HPV 16 E6- and E7-expressing cell lines, CaSki and SiHa, as determined by Western blot analysis.

hWAPL exhibits great potential as a therapeutic target

We previously observed that repression of hWAPL expression by a specific siRNA inhibited cell growth in various cervical cancer-derived cell lines such as SiHa, CaSki (Oikawa *et al*, 2004) and C33A (data not shown) *in vitro*. Thus, we next investigated the possibility that hWAPL might be a novel cancer therapeutic target molecule. We generated tumours in nude mice by subcutaneous injection of SiHa cells. At 1 week after injection of the tumour cells, we measured tumour sizes using caliper squares and then injected siRNA into the tumours on alternate days for 3 weeks (Figure 2A). The growth of tumours injected with the active siRNA specific for *hWAPL* was repressed in comparison with untreated tumours or tumours injected with negative control siRNA (Figure 2A, B). We observed necrosis in the tumours injected with the active siRNA (Figure 2C). In contrast, untreated or control tumours were viable (Figure 2C). We also observed similar effects of the siRNA on tumours arising from another cervical cancer-derived cell line, CaSki (data not shown). These results demonstrate that hWAPL may have potential as a therapeutic target, particularly in cervical cancer.

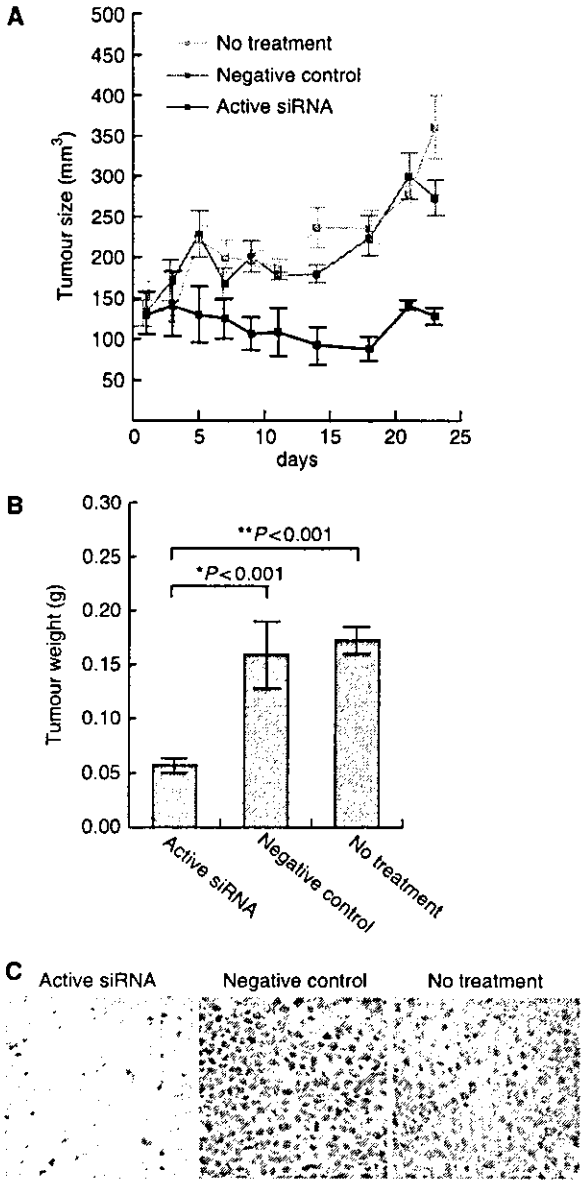

Figure 2 An active siRNA inhibiting hWAPL expression suppressed the growth of subcutaneous tumours derived from SiHa cells inoculated into nude mice. (**A**) Tumour growth curves. The tumour volume (mm^3) was approximated by multiplication of the major axis, the minor axis, and the height of each tumour. Each data point represents the mean of eight samples. Bars, s.e. (**B**) Weights of the tumours in nude mice 25 days after the first siRNA injection. Each data point represents the mean of eight samples. Bars, s.e. $^*P<0.001$ *vs* negative control. $^{**}P<0.001$ *vs* no treatment. (**C**) Representative histology of the subcutaneous tumours in nude mice. The excised tumours were subjected to paraffin sectioning, then stained with haematoxylin and eosin.

However, siRNA itself is rapidly degraded in tumours (Takei *et al*, 2004) and the durability of the effects may be insufficient for clinical application. In fact, although we injected the *hWAPL* siRNA into tumours on alternate days, the repression of the tumour growth was not preserved in a few cases (Figure 2A and data not shown). Recently, a new gene transfer method using atelocollagen has been established (Ochiya *et al*, 1999). Atelocollagen is expected to increase cellular uptake, nuclease resistance, and

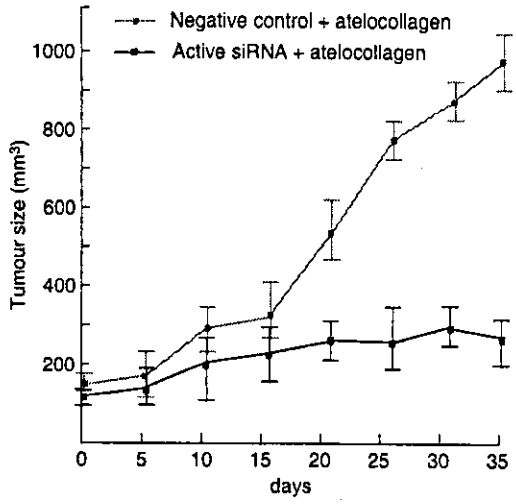

Figure 3 Atelocollagen increases antitumour effects of *hWAPL* siRNA. The growth curves of subcutaneous tumours injected with active or negative control siRNA mixed with atelocollagen were shown. The tumour volume (mm^3) was approximated by multiplication of the major axis, the minor axis, and the height of each tumour. Each data point represents the mean of four samples. Bars, s.e.

prolonged release of siRNAs adiministered into tumours because of its unique property that it is a liquid at 4°C and a gel at 37°C (Ochiya *et al*, 1999; Takei *et al*, 2004). Furthermore, Takei *et al* revealed that atelocollagen contributes the increased stability of siRNAs injected in tumours. Thus, we generated tumours in nude mice by subcutaneous injection of SiHa cells again, and then monitored the growth of the tumours injected with active siRNA or negative control siRNA mixed with atelocollagen (Figure 3). The injection was performed at only 4 time points of 0, 5th, 10th and 20th day for 35 days. As shown in Figure 3, active siRNA with atelocollagen dramatically suppressed tumour growth.

DISCUSSION

Recent findings show that the targeted inactivation of oncogenes could be a specific and effective treatment for cancer (Felsher, 2003). For uterine cervical cancer, HPV E6 and/or E7 were shown to be a strong candidate as a target for gene-specific therapy (Jiang and Milner, 2002; Butz *et al*, 2003; Yoshinouchi *et al*, 2003). However, many subtypes of high-risk HPV have been detected in cervical cancers although HPV types 16 and 18 are great majority of cervical carcinomas (Nakagawa *et al*, 2000). Thus, for clinical application of E6 and E7 siRNAs, various nucleotide sequences may be required for the respective types of HPV. In this study, we have demonstrated that an siRNA of *hWAPL* induces tumour regression *in vivo*. This anticancer effects by the *hWAPL* siRNA stands comparison with the effects of the *E6* siRNA (Jiang and Milner, 2002; Butz *et al*, 2003; Yoshinouchi *et al*, 2003). Therefore, we expect that hWAPL is one of strong candidates as a target for uterine cervical cancer therapy.

ACKNOWLEDGEMENTS

This work was supported in part by Grant-in-Aid for scientific research on Priority Area(C) and Grant-in-Aid for Encouragement of Young Scientists from the Ministry of Education, Scientific, Sports and Culture, and Core Research for Evolutional Science and Technology (CREST) from Japan Science and Technology Corporation.

REFERENCES

Butz K, Ristriani T, Hengstermann A, Denk C, Scheffner M, Hoppe-Seyler F (2003) siRNA targeting of the viral E6 oncogene efficiently kills human papillomavirus-positive cancer cells. *Oncogene* **22**: 5938–5945

Dowhanick JJ, McBride AA, Howley PM (1995) Suppression of cellular proliferation by the papillomavirus E2 protein. *J Virol* **69**: 7791–7799

Dyson N, Guida P, Munger K, Harlow E (1992) Homologous sequences in adenovirus E1A and human papillomavirus E7 proteins mediate interaction with the same set of cellular proteins. *J Virol* **66**: 6893–6902

Felsher DW (2003) Cancer revoked: oncogenes as therapeutic targets. *Nat Rev Cancer* **3**: 375–380

Francis DA, Schmid SI, Howley PM (2000) Repression of the integrated papillomavirus E6/E7 promoter is required for growth suppression of cervical cancer cells. *J Virol* **74**: 2679–2686

Hwang ES, Naeger LK, DiMaio D (1996) Activation of the endogenous p53 growth inhibitory pathway in HeLa cervical carcinoma cells by expression of the bovine papillomavirus E2 gene. *Oncogene* **12**: 795–803

Hwang ES, Riese II DJ, Settleman J, Nilson LA, Honig J, Flynn S, DiMaio D (1993) Inhibition of cervical carcinoma cell line proliferation by the introduction of a bovine papillomavirus regulatory gene. *J Virol* **67**: 3720–3729

Jiang M, Milner J (2002) Selective silencing of viral gene expression in HPV-positive human cervical carcinoma cells treated with siRNA, a primer of RNA interference. *Oncogene* **21**: 6041–6048

Kiyono T, Hiraiwa A, Fujita M, Hayashi Y, Akiyama T, Ishibashi M (1997) Binding of high-risk human papillomavirus E6 oncoproteins to the human homologue of the Drosophila discs large tumor suppressor protein. *Proc Natl Acad Sci USA* **94**: 11612–11616

Munger K, Phelps WC, Bubb V, Howley PM, Schlegel R (1989) The E6 and E7 genes of the human papillomavirus type 16 together are necessary and sufficient for transformation of primary human keratinocytes. *J Virol* **63**: 4417–4421

Nakagawa S, Yoshikawa H, Yasugi T, Kimura M, Kawana K, Matsumoto K, Yamada M, Onda T, Taketani Y (2000) Ubiquitous presence of E6 and E7 transcripts in human papillomavirus-positive cervical carcinomas regardless of its type. *J Med Virol* **62**: 251–258

Naviaux RK, Costanzi E, Haas M, Verma IM (1996) The pCL vector system: rapid production of helper-free, high-titer, recombinant retroviruses. *J Virol* **70**: 5701–5705

Ochiya T, Takahama Y, Nagahara S, Sumita Y, Hisada A, Itoh H, Nagai Y, Terada M (1999) New delivery system for plasmid DNA *in vivo* using atelocollagen as a carrier material: the Minipellet. *Nat Med* **5**: 707–710

Oikawa K, Ohbayashi T, Kiyono T, Nishi H, Isaka K, Umezawa A, Kuroda M, Mukai K (2004) Expression of a novel human gene, human wings apart-like (hWAPL), is associated with cervical carcinogenesis and tumor progression. *Cancer Res* **64**: 3545–3549

Scheffner M, Huibregtse JM, Vierstra RD, Howley PM (1993) The HPV-16 E6 and E6-AP complex functions as a ubiquitin-protein ligase in the ubiquitination of p53. *Cell* **75**: 495–505

Scheffner M, Werness BA, Huibregtse JM, Levine AJ, Howley PM (1990) The E6 oncoprotein encoded by human papillomavirus types 16 and 18 promotes the degradation of p53. *Cell* **63**: 1129–1136

Takei Y, Kadomatsu K, Yuzawa Y, Matsuo S, Muramatsu T (2004) A small interfering RNA targeting vascular endothelial growth factor as cancer therapeutics. *Cancer Res* **64**: 3365–3370

Yoshinouchi M, Yamada T, Kizaki M, Fen J, Koseki T, Ikeda Y, Nishihara T, Yamato K (2003) *In vitro* and *in vivo* growth suppression of human papillomavirus 16-positive cervical cancer cells by E6 siRNA. *Mol Ther* **8**: 762–768

zur Hausen H (1996) Papillomavirus infections – a major cause of human cancers. *Biochim Biophys Acta* **1288**: F55–F78

Alteration of chromosome positioning during adipocyte differentiation

Masahiko Kuroda[1,2,3,*], Hideyuki Tanabe[4,*], Keiichi Yoshida[1,3], Kosuke Oikawa[1,2,3], Akira Saito[5], Tomoharu Kiyuna[6], Hiroshi Mizusawa[7] and Kiyoshi Mukai[1]

[1]Department of Pathology, Tokyo Medical University, 6-1-1 Shinjuku, Shinjuku-ku, Tokyo, 160-8402, Japan
[2]CREST Research Project, Japan Science and Technology Corporation, 4-1-6 Kawaguchi, Saitama, 332-0012, Japan
[3]Shinanomachi Research Park, Keio University, 35 Shinanomachi, Shinjuku-ku, Tokyo, 160-8582, Japan
[4]Department of Biosystems Science, School of Advanced Sciences, The Graduate University for Advanced Studies (Sokendai), Shonan Village, Hayama, Kanagawa 240-0193, Japan
[5]Bioinformatics Business Promotion Department, NEC Corporation, 7-1 Shiba 5-chome, Minato-ku, Tokyo 108-8001, Japan
[6]Fundamental and Environmental Research Laboratories, NEC Corporation, 34 Miyukigaoka, Tsukuba, Ibaraki 305-8501, Japan
[7]Cell bank laboratory, Division of Genetics and Mutagenesis, National Institute of Health Sciences, 1-18-1 Kamiyoga, Setagaya-ku, Tokyo, 158-8501, Japan
*Authors for correspondence (e-mail: kuroda@tokyo-med.ac.jp; tanabe_hideyuki@soken.ac.jp)

Accepted 23 August 2004
Journal of Cell Science 117, 5897-5903 Published by The Company of Biologists 2004
doi:10.1242/jcs.01508

Summary

Chromosomes are highly restricted to specific chromosome territories within the interphase nucleus. The arrangement of chromosome territories is non-random, exhibiting a defined radial distribution as well as a preferential association with specific nuclear compartments, which indicates a functional role for chromosome-territory organization in the regulation of gene expression. In this report, we focus on changes in adipocyte differentiation that are related to a specific chromosomal translocation associated with liposarcoma tumorigenesis, t(12;16). We have examined the relative and radial positioning of the chromosome territories of human chromosomes 12 and 16 during adipocyte differentiation, and detected a close association between the territories of chromosomes 12 and 16 in differentiated adipocytes, an association not observed in preadipocytes. Although further studies are required to elucidate the underlying reasons for the adipocyte-specific translocation of chromosomes 12 and 16, our observations indicate that alteration of relative chromosome positioning might play a key role in the tumorigenesis of human liposarcomas. In addition, these results demonstrate the potential impact of higher order chromatin organization on the epigenetic mechanisms that control gene expression and gene silencing during cell differentiation.

Key words: Chromosome territory, Adipocyte differentiation, TLS-CHOP

Introduction

Chromosomes are not randomly arranged within the interphase nuclei of plant and animal cells; instead, each chromosome occupies its own distinct region, known as a 'territory' (Cremer and Cremer, 2001). The radial organization of chromosome territories has been well-characterized. Typically, gene-poor chromosomes are located in a zone close to the nuclear perimeter, whereas gene-rich chromosomes are found at the center of the nucleus (Boyle et al., 2001; Bridger et al., 2000; Cremer et al., 2003; Cremer and Cremer, 2001; Habermann et al., 2001; Sun et al., 2000; Tanabe et al., 2002a; Tanabe et al., 2002b). We have previously shown that such a gene-density-correlated radial arrangement of chromosome territories is evolutionarily conserved in the genomes of higher primates (Tanabe et al., 2002b). Furthermore, several studies have shown that non-random radial chromosome arrangements are maintained in many different cell types, with the exception of some tumor cells (Boyle et al., 2001). However, because technical limitations render the spatial analysis of chromosome position difficult, it remains unclear whether radial positioning is conserved in all normal cell types.

Specific chromosomal translocations have consistently been found in particular cancers and might promote tumorigenesis through the activation of specific oncogenes or the creation of fusion proteins (Rabbitts, 1994). Human myxoid liposarcomas are associated with the chromosomal translocation t(12;16)(q13.3;p11.2), which creates a chimeric oncogene comprising part of the *TLS/FUS* gene found at 16p11.2 and part of the *CHOP* gene found at 12q13.3 (Aman et al., 1992; Crozat et al., 1993; Eneroth et al., 1990; Rabbitts et al., 1993). The resultant fusion protein is crucial to the transforming activity of the translocation, through its promotion of the unscheduled expression of the adipocyte differentiation gene *DOL54* (Kuroda et al., 1997; Kuroda et al., 1999). The reasons underlying the occurrence of this specific translocation in liposarcomas, however, have remained elusive.

Recent studies have reported that the close juxtaposition of interphase chromosomes plays an important role in such basic cellular processes as gene expression. Moreover, the induction of chromosomal translocations is influenced by proximity of chromosomes, with chromosomes in close proximity to one other presumably more likely to undergo translocations than those that are further apart (Bickmore and Teague, 2002; Parada and Misteli, 2002; Sachs et al., 1997). Interestingly,

such proximity effects have been described in analyses of cancer-causing translocations involved in both leukemia and Ewing sarcoma (Kozubek et al., 1999; Taslerova et al., 2003).

In this study, we examined the relative and radial positioning of human chromosomes 12 and 16 in both preadipocytes and adipocytes to address the question of whether or not chromosome-territory (CT) repositioning occurs during adipocyte differentiation. We observed an alteration in the positioning of these CTs, suggesting that the translocation t(12;16), which might play a key role in liposarcoma tumorigenesis, is induced by the alteration in CT location. In addition, these data indicate that chromatin and nuclear compartments are dynamic during cell differentiation, and that these changes might play a role in the regulation of transcriptional activity in chromatin.

Materials and Methods

Cell culture and adipocyte differentiation

Human preadipocytes were obtained by Zen-Bio from a group of approximately six healthy, non-diabetic, non-obese (body mass index of 25) women (aged 35-38 years) undergoing elective cosmetic liposuction procedures. For adipocyte differentiation, preadipocyte cells were first cultured to confluence in preadipocyte medium (#PM-1; Zen-Bio). Adipocyte differentiation was then induced by replacing the preadipocyte medium with differentiation medium (#DM-2; Zen-Bio). The differentiated adipocyte cells were maintained in adipocyte medium (#AM-1; Zen Bio).

Probe preparation, three-dimensional fluorescence in-situ hybridization and fluorescence detection

In order to obtain three-dimensionally preserved cell nuclei, cells were cultured on coverslip slides and fixed in 4% paraformaldehyde in 0.3× PBS. Permeabilization was performed as previously described (Solovei et al., 2002), by treating the cells with 0.5% Triton X-100 in PBS and then 20% glycerol in PBS, followed by repeated freeze-thaw cycles in liquid nitrogen before a final incubation in 0.1 N HCl.

For the delineation of the human chromosome-12 territory (CT12) and chromosome-16 territory (CT16), we used whole-chromosome painting probes provided by T. Cremer (Ludwig-Maximilians University of Munich, Munich, Germany). Probe labeling was performed by DOP- (degenerated oligonucleotide primer) PCR (Telenius et al., 1992) in the presence of biotin-16-dUTP for human chromosome 12 or digoxigenin-11-dUTP (DIG-11-dUTP) for human chromosome 16 (both from Roche). Three-dimensional fluorescence in-situ hybridization (3D-FISH) and the detection of labeled probes were performed according to protocols described elsewhere (Cremer et al., 2001; Solovei et al., 2002). Briefly, biotinylated human chromosome 12 was detected by avidin-conjugated fluorescein isothiocyanate (FITC) and biotinylated goat-anti-avidin antibody (both from Vector), followed by another round of avidin-FITC binding. Simultaneously, DIG-labeled human chromosome 16 was detected in a similar fashion using a rabbit-anti-DIG antibody (Sigma) and Cy3-labeled goat-anti-rabbit antibody (Amersham Pharmacia Biotech). DNA counterstaining was carried out using TOPRO-3 (Cy5-like fluorescence peak; Molecular Probes), and slides were mounted in Vectashield medium (Vector).

Confocal image

Serial nuclear images were acquired with an axial separation of 200 nm using a confocal laser-scanning microscope (LSM 410; Carl Zeiss) equipped with a 63×/1.4 Plan-Apochromat objective. For each optical section, sequential images were recorded for all three fluorochromes (FITC, Cy3 and Cy5). Stacks of 8-bit grayscale two-dimensional (2D) images were obtained with a pixel size of 66 nm and with 512×512 pixels in each channel. The image stacks were processed with Adobe Photoshop 7 and the distances between fluorescence peak centers (FPCs) were measured after converting image stacks into 256×256 pixels. Three-dimensional (3D) reconstructions of hybridized nuclear image stacks were created using Amira 3.0 TGS (http://www.amiravis.com/) software. Amira software was used only for visualization, not for data analysis.

Segmentation

A probability density of intensity was modeled by a finite normal mixture with m components (m=3 or 4):

$$p(x_j) = \sum_{i=1}^{m} w_i f(x_j \mid \mu_i, \sigma_i) ,$$

where x_j is an intensity value at pixel j, $f(x_j|\mu_i,\sigma_i)$ is the normal density of component i with mean μ_i and standard deviation σ_i, and w_i is a mixture ratio. The parameters (i.e. mixture ratio, intensity mean and standard deviation) were estimated so as to maximize the likelihood using the expectation-maximization (EM) algorithm (Dempster et al., 1977).

Each pixel in 3D space was classified based on a posterior probability $\pi(i,j)$ calculated as:

$$\pi(i,j) = \frac{w_i f(x_j \mid \mu_i, \sigma_i)}{\sum_{k=1}^{m} w_k f(x_j \mid \mu_k, \sigma_k)} .$$

That is, if $\pi(k,j)$ was the largest out of $\pi(i,j)$ (i=1,...,m) then pixel j was classified as a member of component k. Pixels belonging to the component with the largest mean intensity were segmented as nucleus or CT. A threshold was then determined based on the minimum intensity of pixels classified into the largest mean intensity component. To obtain a smooth boundary, an Epanechnikov filter (bandwidth 0.65 μm) was applied to the boundary pixels and their neighboring pixels. The boundary was then resegmented using the threshold determined by the procedure explained above.

Distance measurement

FPCs of the CTs were detected in 3D space. To avoid the effects of local fluctuation, an Epanechnikov filter (bandwidth 0.65 μm) was applied. We defined the pair of chromosomes 12 and 16 with the minimum FPC distance as the proximal pair and the other pair as the distal pair. The distance between CT12 and CT16 of the proximal pair was normalized using the standardized radius of the nucleus. We simulated the distribution of the normalized proximal-pair distances using Monte Carlo simulation (Kozubek et al., 2002) and compared the simulation results with experimental results. The distribution of normalized proximal-pair distances was simulated as follows. First, we generated the radial positions of four FPCs (two for CT12 and two for CT16) in a unit 2D disc using a random-number generator modulated by the experimental radial distributions. Second, the positions were determined assuming a uniform angular distribution (Kozubek et al., 2002). Third, the CT12-CT16 pair with the minimum distance of the two possible combinations was selected and the proximal distance was determined. After 100,000 repetitions, the distributions of the proximal-pair distances were determined.

Normalization of the nucleus size and shape

To remove the effects of size and shape change during cell differentiation, we standardized the nucleus size and shape as follows.

(1) The nucleus area and the FPCs of CT12 and CT16 were projected onto the x-y plane.

(2) The radius of the standard nucleus disc (r_0) was calculated so that the disc area was equal to the projected nucleus area.

(3) The boundary of the original nucleus was extended (or receded) in the 2D plane if the distance from the center of gravity of the nucleus (P_0) to the boundary (R) was shorter (or longer) than the radius of the standard nucleus.

(4) The same transformation was performed on each pixel in a territory region (x) to obtain a deformed position (x'). Radial positions and mutual distances between CTs were evaluated using the values relative to the standardized nucleus radius.

Statistical analysis

We used 38 preadipocyte cells and 41 adipocyte cells for the distance and radial distribution analysis. Welch's t test was used to determine the significance of differences in the proximal-pair distance, and the Kolmogorov-Smirnov (KS) test was applied to the radial distribution differences. The statistical analysis software R version 1.8.1 (http://www.r-project.org/) was used.

Results

Induction of adipocyte differentiation in primary human preadipocyte cells

We cultured human preadipocyte cells until they reached confluence and then induced them to differentiate into adipocyte cells (Fig. 1A,B). The 2D-FISH karyotype of the preadipocyte cells during metaphase appeared normal: $2n$=46, XX, with one pair each of chromosomes 12 and 16 (Fig. 1C).

Relative 3D positioning of the human CT12 and CT16 in preadipocytes and adipocytes

We performed 3D-FISH in 3D-preserved fixed nuclei using painting probes for human chromosomes 12 and 16. Both preadipocyte and adipocyte cells were arrested in the G0/G1 phase in response to cell confluence. Fluorescent signals from both human CT12 and human CT16 were successfully visualized using a two-color analysis, with green and red representing chromosomes 12 and 16, respectively.

We observed the nuclei under a microscope to determine whether or not there was a close association between CT12 and CT16. By visual inspection, we could clearly detect a close association between one CT12 and one CT16 in 81% (33/41) of adipocyte nuclei, whereas this association was observed only in 45% (17/38) of preadipocyte nuclei. Next, we imaged nuclei with a confocal laser-scanning microscope for a more precise quantitative evaluation of the distances between the CTs. A series of optical sections was recorded for each cell, with successive sections separated by an axial distance of 200 nm. All three fluorochromes were recorded sequentially for each section using a box size of 512×512 pixels. A representative z-axis series and 3D reconstruction of both preadipocyte and adipocyte nuclei are displayed in Fig. 2.

For a quantitative evaluation of relative CT positioning, we first measured CT and nucleus size in both preadipocytes and adipocytes (Table 1). We found that the nucleus size was reduced by approximately 10% during adipocyte differentiation. In addition, the CT16 size increased by 50%, whereas the CT12 size showed no significant changes. Furthermore, the nuclei of preadipocyte and adipocyte cells exhibited a range of shapes. Therefore, to eliminate the effects of size and shape change of CTs during cell differentiation, we standardized the nucleus size (Fig. 3). We used the minimum

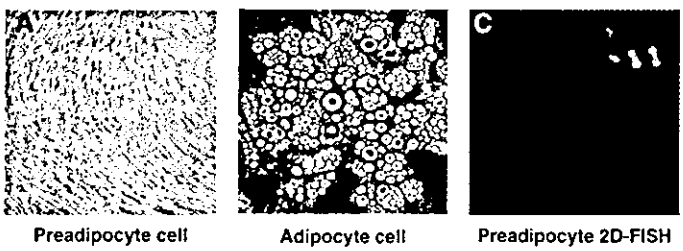

Fig. 1. Induction of adipocyte differentiation in primary human preadipocyte cells. Phase-contrast images (20×) of human preadipocyte cells (A) and matured adipocyte cells (2 weeks after differentiation) (B). (C) A preadipocyte at metaphase in which the DNA has been hybridized with human whole chromosome painting probes for chromosomes 12 (green) and 16 (red).

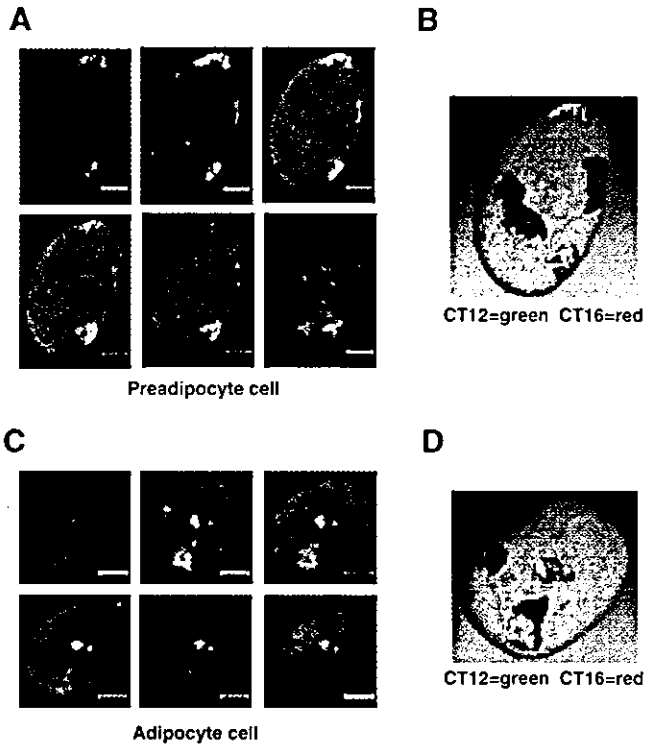

Fig. 2. Visualization of the human chromosome-12 and chromosome-16 territories (CT12 and CT16, respectively). Gallery of 200 nm serial optical sections (every third section is shown: 0 μm, 0.6 μm, 1.2 μm, 1.8 μm, 2.4 μm, 3.0 μm) through a preadipocyte (A) and a mature adipocyte (C) nucleus after 3D-FISH with chromosome painting probes for chromosomes 12 (green) and 16 (red). A DNA counterstain is shown in blue (scale bar, 5 μm). (B,D) 3D reconstructed images of the nuclei presented in A and C, respectively, with outlines of the painted CTs and the nuclear DNA. The adipocyte nucleus displays a proximal association of one CT12 and one CT16 (C,D), whereas the preadipocyte nucleus shows no association between CT12 and CT16 (A,B).

Table 1. Sizes of nuclei and chromosome territories (CTs), showing the means ± s.e.

	Nuclear volume (μm^3)	CT12 volume (μm^3)	CT16 volume (μm^3)
Preadipocyte (n=38)	1147.1±51.8	29.7±2.1	15.3±1.4
Adipocyte (n=41)	1028.9±71.0	29.9±2.4	22.6±1.4

distance between the FPCs of all four possible pairs of CT12 and CT16 in each nucleus as a measure of the level of CT association (Fig. 4A,B). The mean value for the minimum FPC distance relative to the standardized 2D nucleus radius in adipocyte nuclei was significantly smaller than that in preadipocyte nuclei (P=0.016) (Fig. 4C). These results suggest that repositioning of one pair of CTs occurs during adipocyte differentiation. This proximity effect (Fig. 4), as well as the magnification of CT16 (Table 1), substantially increases the probability of an interaction between CT12 and CT16, and is likely to lead to a t(12;16) translocation during adipocyte differentiation. Although the parental origin of this pair of chromosomes is unknown, this raises the intriguing possibility that an association between a specific combination of chromosomes of paternal or maternal origin is established by as yet unknown epigenetic mechanisms.

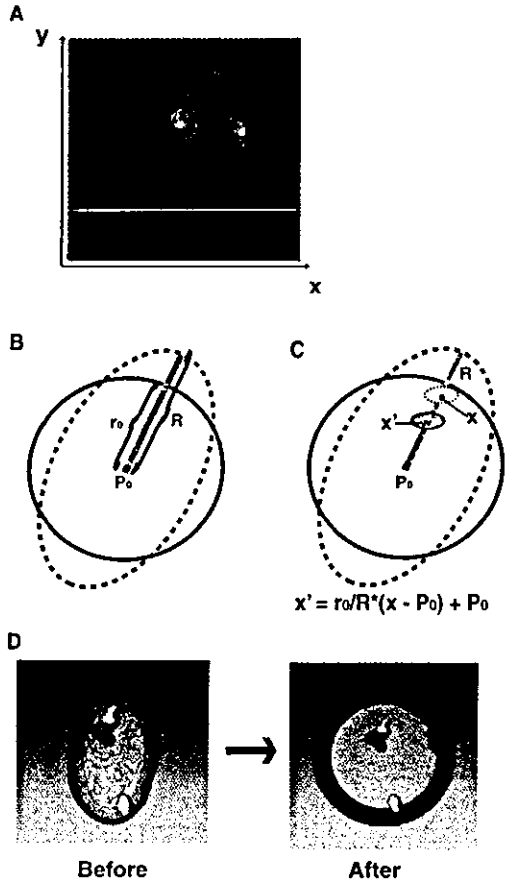

Fig. 3. Topological deformation method for the standardization of cell nuclear shape. (A) Coordinate system of image. The z-axis runs out from the x-y plane towards the reader. (B) Standardization of the nuclear shape. The broken and solid lines indicate actual and standardized nuclear shapes, respectively. (C) Calculation of chromosomal positions. (D) Quasi-3D visualization of the standardized nucleus shape. Deformation was performed in the projected 2D space; transformed x-y positions and the original z position were used. The cylindrical nucleus was constructed using the standardized 2D nucleus shape.

Radial distribution of the CT12 and CT16 does not affect their relative positioning during adipocyte differentiation

Previous studies have showed that the radial rearrangement of genetic structures changes during myogenesis (Chaly and Munro, 1996) and granulopoesis (Bartova et al., 2002; Bartova et al., 2001; Bartova et al., 2000b). Therefore, we next examined the radial distributions of CT12 and CT16 in preadipocyte and adipocyte cells. We investigated total radial distributions over the standardized 2D nucleus and compared them for the cell types studied using the KS test. Although there were no significant differences between CT12 and CT16 during adipocyte differentiation, the means of the total radial distribution appeared to shift towards the center for CT16 (from $\langle r \rangle$=59.0±22.0 to 56.8±21.5, P>0.49, where $\langle r \rangle$ stands for the mean radial position) and the mean of the total radial distribution for CT12 shifted toward the periphery (from $\langle r \rangle$=57.7±21.4 to 0.59.8±21.4, P>0.7) (Fig. 5). This shift of the CT might account for the reduction in relative distances between CT12 and CT16.

Thus, to determine whether the difference of minimum FPC distances described above was affected by the fluctuation of the radial distribution of CT12 and CT16 during cell differentiation, we conducted a Monte Carlo simulation (Kozubek et al., 2002). The minimum distances obtained through the simulation were not significantly different (0.45±0.25 for adipocyte and 0.46±0.26 for preadipocyte). Thus, the change in distance between CT12 and CT16 during adipocyte differentiation was not caused by changes in radial distributions.

Discussion

Insight into the epigenetic function of CT repositioning is important for understanding how nuclear architecture is organized in different cell types, and how it might be involved in cell differentiation and tumorigenesis (Cremer and Cremer, 2001; Jenuwein and Allis, 2001; Strahl and Allis, 2000). There are two aspects to consider with respect to CT positioning: the absolute radial location within the nucleus and the position of CTs relative to one another (Parada and Misteli, 2002). The radial location of a CT is tightly correlated with its size and gene density. As a general rule, gene-dense CTs are found near the center of the nucleus, whereas gene-poor CTs localize to the periphery of the nucleus (Boyle et al., 2001; Cremer et al., 2001; Croft et al., 1999). This rule is applicable in cells with spherical nuclei, such as lymphocytes and lymphoblastoid cell lines, and its evolutionary conservation has been clearly demonstrated (Tanabe et al., 2002b). By contrast, the extent to which the rule applies to cell types with non-spherical nuclei, such as fibroblasts, epithelial cells and tumor cell lines, remains controversial (Boyle et al., 2001; Bridger et al., 2000; Cremer et al., 2003; Cremer et al., 2001; Croft et al., 1999; Kozubek et al., 2002; Tanabe et al., 2002b).

In this study, we evaluate the arrangement of CT12 and CT16 in preadipocyte and adipocyte cells. Interestingly, we

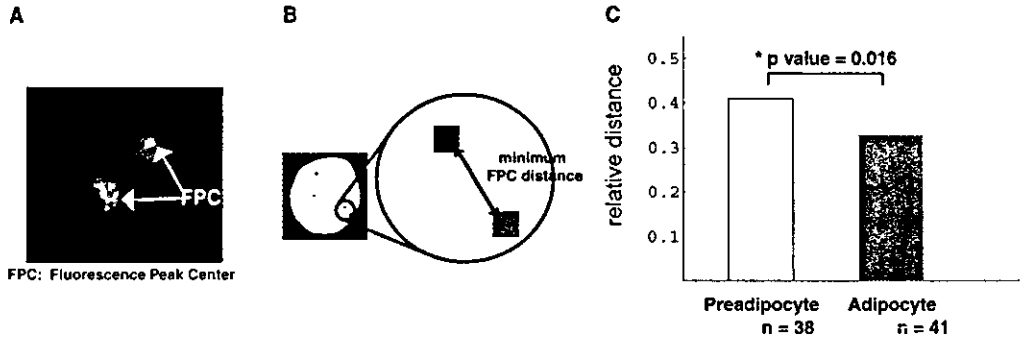

Fig. 4. Relative positions of human chromosome-12 and chromosome-16 territories (CT12 and CT16, respectively). (A) The definition of a representative peak point for a CT. Green dots indicate the fluorescence peak center (FPC). The location of the CT is represented by the position of its FPC. (B) Schema of the minimum FPC distance. We measured the pixel-to-pixel distance between the FPCs of CT12 and CT16, and then recorded the shortest of the four distances obtained from the four possible pairings as the minimum FPC distance. (C) Quantitative evaluation of the minimum FPC distance between CT12 and CT16. The distances are normalized using the radius of the standardized 2D nucleus. The significance of the difference between minimum FPC distances in preadipocytes and adipocytes was evaluated using the Welch's *t* test (P=0.017).

observed that the minimum FPC distance of CT12 and CT16 changed during adipogenesis. Furthermore, we examined whether or not the total radial distribution of CT12 and CT16 changed during adipogenesis. We could not detect a significant radial shift between the two cell types using the KS test (Fig. 5). Thus, we conclude that the relative positioning of CT12 and CT16 was altered in during adipogenesis. The reasons for the difference in behavior between chromosomes 12 and 16 are at present unknown. However, it is possible that the difference is due to variations in local gene expression from each chromosome.

The process of cellular differentiation represents a remarkably coordinated program of gene regulation that directs multipotent stem-cell precursors down various lineages into fully mature and functionally distinct cell types. During adipocyte differentiation, many genes have been shown to be regulated in a differentiation-dependent manner. It is has been clearly shown that adipogenic transcription factors such as C/EBP and PPAR play an important role in the regulation of gene expression through conventional genetic mechanisms. However, recent reports indicate that the spatial arrangement of chromatin in the nucleus is correlated with cell differentiation (Bartova et al., 2002; Bartova et al., 2001; Bartova et al., 2000a; Manuelidis, 1990). Moreover, gene positioning and heterochromatin-mediated gene silencing appear to play an important role in cell differentiation (Bartova et al., 2002). Our results and other studies of CTs (Mahy et al., 2002a; Mahy et al., 2002b) suggest that chromosome distribution might also control epigenetic mechanisms that affect regulation of genes. Thus, changes in CT location might act as an epigenetic factor that functions on a different level than the genetic code.

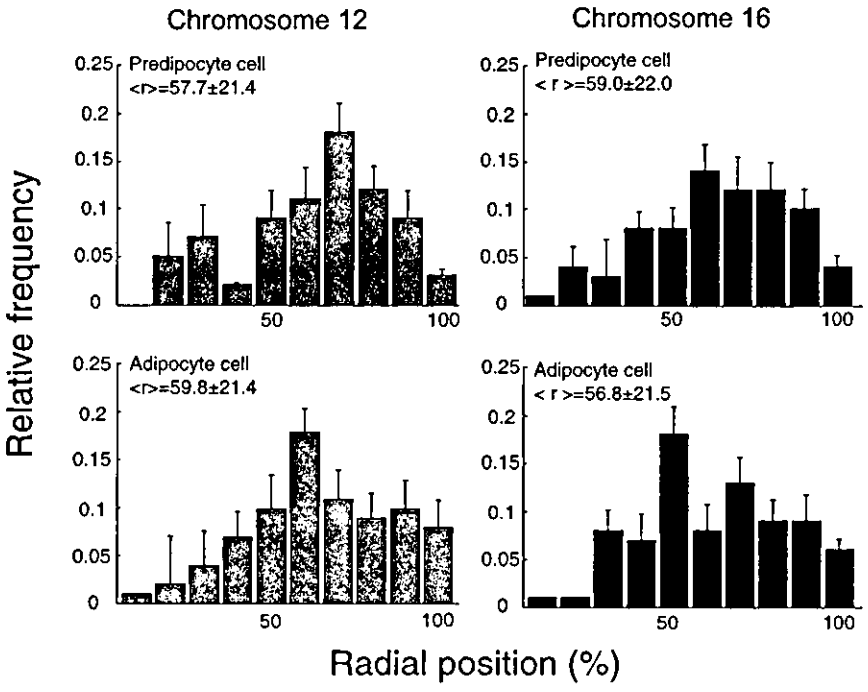

Fig. 5. Radial positions of human chromosome-12 and chromosome-16 territories (CT12 and CT16, respectively). Total radial distributions of CT12 and CT16 over the standardized 2D nucleus (n=76=38×2 for preadipocyte, and n=82=41×2 for adipocyte). The mean values (<r>) and standard errors of all distributions are also shown.

The relative positioning of CTs with respect to one other is known to influence the translocation frequencies between two chromosomes. For example, human myxoid and round cell liposarcomas are associated with specific chromosomal translocations (Sreekantaiah et al., 1992). The *TLS-CHOP* fusion gene derived from t(12;16) is present in 95-98% of myxoid and round cell liposarcomas but, in rare cases, a variant t(12;22) translocation is observed that results in the *EWS-CHOP* fusion gene (Hosaka et al., 2002). The TLS-CHOP chimeric protein has transforming activity (Kuroda et al., 1997) and induces the expression of the *DOL54* gene, which is normally associated with adipocyte differentiation (Kuroda et al., 1999). In addition, histological diagnosis of myxoid liposarcomas reveals the presence of immature adipose cells called lipoblasts, suggesting that myxoid liposarcomas come from an immature mesechymal or adipocytic cell lineage. However, it is still unknown why the chromosomal translocation t(12;16)(q13.3;p11.2) and the creation of the *TLS-CHOP* fusion gene occur specifically in liposarcomas. Our observations demonstrate that the minimum FPC distance between CT12 and CT16 is reduced, and the size of CT16 is magnified during adipocyte differentiation. These phenomena might lead to the t(12;16) translocation event specific to liposarcomas.

In conclusion, we have demonstrated that the particular CTs involved in a specific translocation event implicated in cancer development can physically associate with one another following differentiation in human cell lines. These results also suggest that the t(12;16) translocation, which has been implicated in liposarcoma tumorigenesis, occurs because of an alteration in chromosome location.

We thank T. Cremer (Ludwig-Maximilians University of Munich, Munich, Germany) for providing the human painting probes and S. Wagstaff (NEC, Bio-IT) for preparing the Amira 3D-reconstructed images and other helpful assistance. This study was supported in part by a Grant-in-Aid for scientific research on Priority Area (C) from the Ministry of Education, Science, Sports and Culture, a grant from Core Research for Evolutional Science and Technology (CREST), Japan Science and Technology Corporation, Health Sciences Research Grants, Ministry of Health, Labor and Welfare, Japan, and a grant from Japan Health Sciences Foundation.

References

Aman, P., Ron, D., Mandahl, N., Fioretos, T., Heim, S., Arheden, K., Willen, H., Rydholm, A. and Mitelman, F. (1992). Rearrangement of the transcription factor gene *CHOP* in myxoid liposarcomas with t(12;16)(q13;p11). *Genes Chromosomes Cancer* **5**, 278-285.

Bartova, E., Kozubek, S., Kozubek, M., Jirsova, P., Lukasova, E., Skalnikova, M. and Buchnickova, K. (2000a). The influence of the cell cycle, differentiation and irradiation on the nuclear location of the *ABL*, *BCR* and c-*MYC* genes in human leukemic cells. *Leuk. Res.* **24**, 233-241.

Bartova, E., Kozubek, S., Kozubek, M., Jirsova, P., Lukasova, E., Skalnikova, M., Cafourkova, A. and Koutna, I. (2000b). Nuclear topography of the c-*MYC* gene in human leukemic cells. *Gene* **244**, 1-11.

Bartova, E., Kozubek, S., Jirsova, P., Kozubek, M., Lukasova, E., Skalnikova, M., Cafourkova, A., Koutna, I. and Pasekova, R. (2001). Higher-order chromatin structure of human granulocytes. *Chromosoma* **110**, 360-370.

Bartova, E., Kozubek, S., Jirsova, P., Kozubek, M., Gajova, H., Lukasova, E., Skalnikova, M., Ganova, A., Koutna, I. and Hausmann, M. (2002). Nuclear structure and gene activity in human differentiated cells. *J. Struct. Biol.* **139**, 76-89.

Bickmore, W. A. and Teague, P. (2002). Influences of chromosome size, gene density and nuclear position on the frequency of constitutional translocations in the human population. *Chromosome Res.* **10**, 707-715.

Boyle, S., Gilchrist, S., Bridger, J. M., Mahy, N. L., Ellis, J. A. and Bickmore, W. A. (2001). The spatial organization of human chromosomes within the nuclei of normal and emerin-mutant cells. *Hum. Mol. Genet.* **10**, 211-219.

Bridger, J. M., Boyle, S., Kill, I. R. and Bickmore, W. A. (2000). Re-modelling of nuclear architecture in quiescent and senescent human fibroblasts. *Curr. Biol.* **10**, 149-152.

Chaly, N. and Munro, S. B. (1996). Centromeres reposition to the nuclear periphery during L6E9 myogenesis in vitro. *Exp. Cell Res.* **223**, 274-278.

Cremer, M., von Hase, J., Volm, T., Brero, A., Kreth, G., Walter, J., Fischer, C., Solovei, I., Cremer, C. and Cremer, T. (2001). Non-random radial higher-order chromatin arrangements in nuclei of diploid human cells. *Chromosome Res.* **9**, 541-567.

Cremer, M., Kupper, K., Wagler, B., Wizelman, L., von Hase, J., Weiland, Y., Kreja, L., Diebold, J., Speicher, M. R. and Cremer, T. (2003). Inheritance of gene density-related higher order chromatin arrangements in normal and tumor cell nuclei. *J. Cell Biol.* **162**, 809-820.

Cremer, T. and Cremer, C. (2001). Chromosome territories, nuclear architecture and gene regulation in mammalian cells. *Nat. Rev. Genet.* **2**, 292-301.

Croft, J. A., Bridger, J. M., Boyle, S., Perry, P., Teague, P. and Bickmore, W. A. (1999). Differences in the localization and morphology of chromosomes in the human nucleus. *J. Cell Biol.* **145**, 1119-1131.

Crozat, A., Aman, P., Mandahl, N. and Ron, D. (1993). Fusion of CHOP to a novel RNA-binding protein in human myxoid liposarcoma. *Nature* **363**, 640-644.

Dempster, A. P., Laird, N. M. and Rubin, D. B. (1977). Maximum likelihood from incomplete data via the EM algorithm. *J. Roy. Stat. Soc.* **39**, 1-38.

Eneroth, M., Mandahl, N., Heim, S., Willen, H., Rydholm, A., Alberts, K. A. and Mitelman, F. (1990). Localization of the chromosomal breakpoints of the t(12;16) in liposarcoma to subbands 12q13.3 and 16p11.2. *Cancer Genet. Cytogenet.* **48**, 101-107.

Habermann, F. A., Cremer, M., Walter, J., Kreth, G., von Hase, J., Bauer, K., Wienberg, J., Cremer, C., Cremer, T. and Solovei, I. (2001). Arrangements of macro- and microchromosomes in chicken cells. *Chromosome Res.* **9**, 569-584.

Hosaka, T., Nakashima, Y., Kusuzaki, K., Murata, H., Nakayama, T., Nakamata, T., Aoyama, T., Okamoto, T., Nishijo, K., Araki, N. et al. (2002). A novel type of *EWS-CHOP* fusion gene in two cases of myxoid liposarcoma. *J. Mol. Diagn.* **4**, 164-171.

Jenuwein, T. and Allis, C. D. (2001). Translating the histone code. *Science* **293**, 1074-1080.

Kozubek, S., Lukasova, E., Mareckova, A., Skalnikova, M., Kozubek, M., Bartova, E., Kroha, V., Krahulcova, E. and Slotova, J. (1999). The topological organization of chromosomes 9 and 22 in cell nuclei has a determinative role in the induction of t(9,22) translocations and in the pathogenesis of t(9,22) leukemias. *Chromosoma* **108**, 426-435.

Kozubek, S., Lukasova, E., Jirsova, P., Koutna, I., Kozubek, M., Ganova, A., Bartova, E., Falk, M. and Pasekova, R. (2002). 3D structure of the human genome: order in randomness. *Chromosoma* **111**, 321-331.

Kuroda, M., Ishida, T., Takanashi, M., Satoh, M., Machinami, R. and Watanabe, T. (1997). Oncogenic transformation and inhibition of adipocytic conversion of preadipocytes by TLS/FUS-CHOP type II chimeric protein. *Am. J. Pathol.* **151**, 735-744.

Kuroda, M., Wang, X., Sok, J., Yin, Y., Chung, P., Giannotti, J. W., Jacobs, K. A., Fitz, L. J., Murtha-Riel, P., Turner, K. J. et al. (1999). Induction of a secreted protein by the myxoid liposarcoma oncogene. *Proc. Natl. Acad. Sci. USA* **96**, 5025-5030.

Mahy, N. L., Perry, P. E. and Bickmore, W. A. (2002a). Gene density and transcription influence the localization of chromatin outside of chromosome territories detectable by FISH. *J. Cell Biol.* **159**, 753-763.

Mahy, N. L., Perry, P. E., Gilchrist, S., Baldock, R. A. and Bickmore, W. A. (2002b). Spatial organization of active and inactive genes and noncoding DNA within chromosome territories. *J. Cell Biol.* **157**, 579-589.

Manuelidis, L. (1990). A view of interphase chromosomes. *Science* **250**, 1533-1540.

Parada, L. and Misteli, T. (2002). Chromosome positioning in the interphase nucleus. *Trends Cell Biol.* **12**, 425-432.

Rabbitts, T. H. (1994). Chromosomal translocations in human cancer. *Nature* **372**, 143-149.

Rabbitts, T. H., Forster, A., Larson, R. and Nathan, P. (1993). Fusion of

the dominant negative transcription regulator *CHOP* with a novel gene *FUS* by translocation t(12;16) in malignant liposarcoma. *Nat. Genet.* **4**, 175-180.

Sachs, R. K., Chen, A. M. and Brenner, D. J. (1997). Review: proximity effects in the production of chromosome aberrations by ionizing radiation. *Int. J. Radiat. Biol.* **71**, 1-19.

Solovei, I., Walter, J., Cremer, M., Habermann, F., Schermelleh, L. and Cremer, T. (2002). FISH on three-dimensionally preserved nuclei. In *FISH: A Practical Approach* (ed. B. Beatty, S. Mai and J. Squire), pp. 119-157. Oxford, UK: Oxford University Press.

Sreekantaiah, C., Karakousis, C. P., Leong, S. P. and Sandberg, A. A. (1992). Cytogenetic findings in liposarcoma correlate with histopathologic subtypes. *Cancer* **69**, 2484-2495.

Strahl, B. D. and Allis, C. D. (2000). The language of covalent histone modifications. *Nature* **403**, 41-45.

Sun, H. B., Shen, J. and Yokota, H. (2000). Size-dependent positioning of human chromosomes in interphase nuclei. *Biophys. J.* **79**, 184-190.

Tanabe, H., Habermann, F. A., Solovei, I., Cremer, M. and Cremer, T. (2002a). Non-random radial arrangements of interphase chromosome territories: evolutionary considerations and functional implications. *Mutat. Res.* **504**, 37-45.

Tanabe, H., Muller, S., Neusser, M., von Hase, J., Calcagno, E., Cremer, M., Solovei, I., Cremer, C. and Cremer, T. (2002b). Evolutionary conservation of chromosome territory arrangements in cell nuclei from higher primates. *Proc. Natl. Acad. Sci. USA* **99**, 4424-4429.

Taslerova, R., Kozubek, S., Lukasova, E., Jirsova, P., Bartova, E. and Kozubek, M. (2003). Arrangement of chromosome 11 and 22 territories, *EWSR1* and *FLI1* genes, and other genetic elements of these chromosomes in human lymphocytes and Ewing sarcoma cells. *Hum. Genet.* **112**, 143-155.

Telenius, H., Carter, N. P., Bebb, C. E., Nordenskjold, M., Ponder, B. A. and Tunnacliffe, A. (1992). Degenerate oligonucleotide-primed PCR: general amplification of target DNA by a single degenerate primer. *Genomics* **13**, 718-725.